Peptide-TLR-7/8 agonist conjugate vaccines chemically programmed for nanoparticle self-assembly enhance the breadth of CD8 T cell immunity to tumor neoantigens

Geoffrey M. Lynn[1,2 †]*, Christine Sedlik[3,4 †], Faezzah Baharom[1], Yaling Zhu[2], Andrei Ramirez-Valdez[1], Vincent L. Coble[2], Neeha Zaidi[1], Kennedy Tobin[1], Nicholas Blobel[1], Jordan Denizeau[3,4], Philippe de la Rochere[3,4], Brian J. Francica[5,9], Brennan Decker[2], Mateusz Maciejewski[2], Justin Cheung[1], Hidehiro Yamane[1], Margery G. Smelkinson[6], Joseph R. Francica[1], Richard Laga[7], Joshua D. Bernstock[2], Leonard W. Seymour[8], Charles G. Drake[5,9], Olivier Lantz[3,4], Eliane Piaggio[3,4], Andrew S. Ishizuka[1,2 ‡], and Robert A. Seder[1 ‡]*

[1] Vaccine Research Center (VRC), National Institute of Allergy and Infectious Diseases (NIAID), National Institutes of Health (NIH), Bethesda, MD, USA

[2] Avidea Technologies, Inc., Baltimore, MD, USA

[3] Institut Curie, PSL Research University, INSERM U932, Paris, France

[4] Centre d'Investigation Clinique Biothérapie, Institut Curie, Paris, France

[5] Sidney Kimmel Comprehensive Cancer Center, Johns Hopkins University, Baltimore, MD, USA

[6] Biological Imaging Section, Research Technologies Branch, NIAID, NIH, Bethesda, MD, USA

[7] Institute of Macromolecular Chemistry, Academy of Sciences of the Czech Republic, Prague, Czech Republic

[8] Department of Oncology, University of Oxford, Oxford, United Kingdom

[9] Present addresses: Aduro Biotech, Berkeley, CA (B.J.F.), Herbert Irving Comprehensive Cancer Center, Columbia University Medical Center, New York, NY, USA (C.G.D.)

[†] These authors contributed equally to this work

[‡] These authors jointly supervised this work

* Corresponding authors

Geoffrey M. Lynn (geoffrey.lynn@avideatechnologies.com)

Robert A. Seder (rseder@mail.nih.gov)

ABSTRACT

Advances in genomic sequencing and *in silico* prediction algorithms have enabled the development of personalized cancer vaccines (PCVs) targeting tumor-specific neoantigens. With current peptide- and RNA-based PCVs, only ~10% of predicted neoantigens induce *de novo* CD8 T cell responses. Here, we show that the efficiency for inducing CD8 T cells with peptide-based PCVs can be markedly improved but is highly dependent on the physical form of the peptide antigen. Particulate peptide antigens, unlike soluble peptide antigens, are efficiently taken up by dendritic cells in lymphoid tissue and promote CD8 T cell expansion. However, the broad range of neoantigen physicochemical properties is a major challenge to ensuring consistent particle formulations with peptide-based PCVs. Therefore, we developed a PCV platform based on charge-modified peptide-TLR-7/8 agonist conjugates that are chemically programmed for self-assembling into nanoparticles ("SNP-7/8a") of a defined size (20–50 nm) irrespective of the underlying neoantigen composition. Bioinformatics analysis of 72 million human genome-derived neoantigens was used to demonstrate that SNP-7/8a ensures consistent nanoparticle formation with neoantigens at extremes of charge and hydropathy. Vaccination of mice with SNP-7/8a using predicted neoantigens (n = 179) from three tumor models induced CD8 T cells against ~50% of those with high predicted MHC-I binding affinity (IEDB consensus score < 0.5). Therapeutic vaccination with SNP-7/8a enhanced tumor clearance. Charge-modified conjugates are a universal approach for co-delivering peptide antigens and adjuvants in nanoparticles to enhance anticancer T cell immunity.

INTRODUCTION

Mutations in tumor DNA lead to the expression of altered self-proteins that may be processed into short peptide fragments capable of binding MHC molecules on the surface of cancer cells[1]. T cells that recognize MHC-bound mutant peptides ("neoantigens")[2] are highly effective for mediating tumor-specific killing and have been shown to promote durable tumor regression and prolonged survival of patients with advanced cancers[3,4]. Additionally, improved survival of patients treated with checkpoint inhibitors (CPIs), such as anti-PD-1 and anti-CTLA-4, correlates with tumor mutational load[5,6] and T cell infiltration into tumors[7]. Based on these findings, personalized cancer vaccines (PCVs) that generate neoantigen-specific T cells are being actively developed as cancer treatment modalities[8-11].

The feasibility of using peptide- and RNA-based PCVs has been demonstrated in both mice[12,13] and humans[14,15]. While these studies have established an important proof-of-concept, a potential challenge with current PCV approaches is their efficiency for generating neoantigen-specific CD8 T cells *in vivo*. For example, less than 10% of 184 predicted neoantigens derived from 3 mouse tumor lines included in either peptide- or RNA-based PCVs induced detectable CD8 T cell responses, even though the putative neoantigens were selected on the basis of high predicted binding affinity for MHC-I[13]. Moreover, patients who received peptide neoantigens combined with the adjuvant polyICLC had low to undetectable CD8 T responses when assessed directly *ex vivo* from blood[14]. Based on current cost and manufacturing constraints that restrict the number of predicted neoantigens that can be included in PCVs[10], as well as the limited number of neoantigens in patients with low mutational burden tumors[16], more efficient neoantigen prediction and/or vaccination approaches are likely needed.

The focus of this study was to determine whether the magnitude and breadth of CD8 T cell responses to neoantigens could be improved by optimization of a peptide-based PCV formulation. We evaluated how a number of peptide vaccine properties (*e.g.*, peptide length, hydrophobicity, charge and physical form) impact immunogenicity *in vivo*. The data presented herein show that the physical form of the peptide antigen is a key determinant of immunogenicity: peptide antigens in a particle form induced significantly higher CD8 T cell responses than soluble peptide antigens when administered with various TLR agonists (TLRa) used as adjuvants.

Various particle vaccine delivery technologies have been developed to enhance T cell immunogenicity to peptide antigens[17-21]; however, the broad variability of neoantigen physicochemical properties that arise from amino acid sequence variation may limit the translatability and scalability of such technologies for use as PCVs. Indeed, formulating peptide antigens and adjuvants with commonly used particle technologies, including poly(lactic-co-glycolic acid) (PLGA)[22,23], liposomes[24], polymersomes[25] and emulsions[26,27], can be an empirical process whereby peptide loading and formulation characteristics may be different for each antigen. An alternative approach is to use conjugate vaccines based on peptide antigens linked to hydrophobic carriers (*e.g.*, lipids[28], fatty acids[29] and TLRa[30,31]) that can induce particle assembly or bind albumin for more efficient delivery to lymph nodes[28,32]. Conjugate vaccines offer the potential advantages that antigen loading is chemically defined and that adjuvants can be covalently attached to ensure co-delivery of both components to antigen presenting cells (APCs), which may be needed for optimal T cell priming[33,34]. A major limitation of these current particle and conjugate vaccine technologies, however, is that they do not account for the broad range of neoantigen properties, which can lead to formulation variability, including the propensity of

hydrophobic peptides to form aggregates that complicate manufacturing and form injection-site depots that can lead to sub-optimal CD8 T cell immunity[35-37].

To overcome these limitations, we developed a PCV platform based on charge-modified peptide-TLR-7/8a conjugates that enable reproducible and precise loading of diverse peptide neoantigens with TLR-7/8a in self-assembling nanoparticles (SNP-7/8a) of a defined size (20–50 nm). The data reported here show that SNP-7/8a overcomes several manufacturing limitations of current peptide-based PCVs and leads to expanded breadth and magnitude of neoantigen-specific CD8 T cells as well as improved tumor clearance.

RESULTS

Peptide physical form is a key determinant of CD8 T cell immunogenicity

Synthetic long peptides (LPs) consisting of 20–40 amino acid sequences, which often include an 8–11 amino acid minimal CD8 T cell epitope ("Min"), combined with various adjuvants have been widely studied as cancer vaccines in pre-clinical and clinical settings[38-40]. However, it is not well understood how differences in the amino acid composition, which determines the physical form (*i.e.*, hydrodynamic behavior)[41] of LPs, affects T cell immunogenicity.

To determine how peptide physical form impacts CD8 T cell immunogenicity, the MHC-I epitope from ovalbumin (SIINFEKL) was used as a model immunogen and synthesized either as a hydrophobic 30-amino acid peptide that is particulate in aqueous buffer ("LSP") or as a hydrophilic version containing several mutations in the region adjacent to the SIINFEKL epitope ("LSS", **Fig. 1a**). The LPs were then either admixed with a particle TLR-7/8a (PP-7/8a)[42] or covalently attached to a TLR-7/8a and administered to mice (**Fig. 1a** and **Extended Data Fig. 1a**).

Vaccination with the Particle LPs (LSP mixed with PP-7/8a or LSP-7/8a) led to 20-fold higher CD8 T cell responses as compared with vaccination with the Soluble LPs (LSS mixed with PP-7/8a or LSS-7/8a; **Fig. 1b**). Moreover, LSP admixed with either CpG (TLR-9a) or polyICLC (TLR-3a) induced ~10-fold higher magnitude CD8 T cell responses and improved survival following challenge with ovalbumin-expressing B16 tumor cells (B16.OVA) as compared with LSS combined with the same adjuvants (**Extended Data Fig. 1b–d**).

As a possible mechanism to account for the above findings, we determined that antigen-specific CD8 T cells in mice that received the Particle LP expanded for up to 1 week after vaccination and underwent a greater number of cell divisions as compared with CD8 T cells in mice immunized with the Soluble LP (**Fig. 1c** and **Extended Data Fig. 2**). Additionally, the Particle LP had higher uptake by CD11c+ dendritic cells (DCs) and was retained longer in draining lymph nodes compared with the Soluble LP (**Fig. 1d**,**e**). Together, these data suggest that Particle LPs enhance CD8 T cell responses through prolonged antigen presentation resulting from increased peptide uptake by DCs in draining lymph nodes.

To extend these findings to PCVs, we evaluated the relationship between peptide physical form and immunogenicity using two neoantigens, Reps1 and Irgq, from the mouse tumor cell line MC38. While these neoantigens are known to bind MHC-I, they were previously reported to be immunogenic and "non-immunogenic," respectively, when administered as LP mixed with the adjuvants polyIC and CD40 agonist[12]. Here, we show that Reps1 LP is particulate in aqueous solution and induces high magnitude CD8 T cell responses when admixed with a variety of adjuvants (*i.e.*, PP-7/8a, CpG, or polyICLC), whereas Irgq LP is water-soluble and induces low to undetectable CD8 T cell responses (**Fig. 1f** and **Extended Data Fig. 3**). The physical form of each neoantigen was altered by swapping the amino acid residues flanking each

minimal epitope to produce chimeric Reps1, which is soluble, and chimeric Irgq, which is particulate. For each of the adjuvants evaluated, the Irgq chimer induced significantly higher CD8 T cell responses than the native soluble form, whereas the Reps1 chimer did not induce responses significantly above background (**Fig. 1f** and **Extended Data Fig. 3**).

The above studies were performed with chimeric peptides wherein amino acids adjacent to each minimal epitope were modified, which may have affected intracellular processing. To more directly isolate how peptide physical form impacts CD8 T cell responses without modifying the native peptide neoantigen sequence, we directly attached either the native LP (26-mer) or Min (9-mer) Irgq sequence to a hydrophobic oligopeptide-TLR-7/8a that induces microparticle (MP-7/8a) formation in aqueous conditions and assessed immunogenicity *in vivo*. While the water-soluble native Irgq LP admixed with adjuvants was non-immunogenic (**Fig. 1f**), both the native LP and Min Irgq sequences induced high magnitude CD8 T cell responses when rendered particulate through direct attachment to a particle-forming adjuvant (**Fig. 1g**). These data substantiate that particulate delivery of peptide antigens, including neoantigens, is critical for inducing high magnitude CD8 T cell responses.

Self-assembling nanoparticles based on charged-modified peptide-TLR-7/8a conjugates (SNP-7/8a)

To enable precise loading of peptide antigens and TLR-7/8a in particles with reproducible formulation characteristics, we developed a modular and chemically tunable vaccine platform based on charge-modified (CM) conjugates comprising peptide antigens linked to both a charge modifying group and a hydrophobic block through enzyme degradable linkers at the N- and C- termini of the peptide, respectively (**Fig. 2a**). Upon resuspension in aqueous solution, the hydrophobic block promotes multimerization while the charge-modifying group

provides a countervailing force that induces formation of nanoparticle micelles (20–50 nm) and thereby prevents the formation of large microparticles or aggregates that can result from conjugates without charge modification (**Fig 2b**). To ensure biocompatibility and manufacturing scalability, charge-modifying groups based on charged amino acids and hydrophobic blocks (referred to as oligo-7/8a) based on biodegradable oligopeptides linked to a precise number of small molecule TLR-7/8a were used. Thus, these CM conjugates are molecularly-defined single molecules that are chemically programmed via the charge-modifying group and hydrophobic block to self-assemble into nanoparticles co-delivering peptide neoantigens and TLR-7/8a (SNP-7/8a; **Fig. 2a**).

Net charge of CM conjugates determines SNP formation

It was unknown *a priori* what magnitude of charge would be required to stabilize and ensure reproducible formulations of nanoparticles formed by CM conjugates with different neoantigens. Therefore, we systematically investigated how modulating the net charge of CM conjugates impacts particle size. Evaluation of 35 CM conjugates with various charge-modifying groups appended to the N-terminus of the same peptide neoantigen revealed an inverse relationship between the magnitude of CM conjugate net charge and particle size (**Fig. 2c**). This inverse relationship between magnitude of charge and particle size was confirmed with an additional 746 unique CM conjugates with a variety of antigen sequences, wherein ~90% of CM conjugates having a net absolute charge > 5 assembled into ~20–50 nm nanoparticle micelles (**Fig. 2d**).

Based on this data set, a random forest machine learning (ML) model[43] was used to predict how CM conjugate properties impact the hydrodynamic behavior of SNP-7/8a. This approach used the underlying physical properties of each CM conjugate to predict whether a

given composition would form stable nanoparticles (as measured by turbidity < 0.05) or unstable, larger particles (turbidity > 0.05) with a mean ROC AUC of 0.90 (**Fig. 2e**). Analysis of the underlying ML model revealed that CM conjugate net charge and hydropathy were relatively important features determining nanoparticle formation, whereas peptide antigen length and hydrophobic block composition were less important (**Fig. 2f**).

To extend these findings, the impact of net charge on the size of particles formed by CM conjugates comprising common hydrophobic carrier molecules (fatty acids, cholesterol, and lipids; **Fig. 2g**) and hydrophobic oligopeptides linked to agonists of other pattern recognition receptors (TLR-2/6, TLR-4, TLR-7, NLR, and STING; **Fig 2h**) was determined. These data show an inverse relationship between CM conjugate net charge and particle size, which was independent of the hydrophobic block composition.

SNP-7/8a parameters that affect T cell induction

In vivo structure-activity relationship studies were performed to evaluate how linker composition (cathepsin[44] and proteasomal[45] processing sites), TLR-7/8a potency and number, and type of charge (*i.e.*, positive versus negative net charge) impact CD8 T cell responses by CM conjugates. Cathepsin degradable linkers placed between the peptide neoantigen and both the charge-modifying group and hydrophobic block increased the efficiency of antigen presentation *in vitro* and led to significantly higher CD8 T cell responses *in vivo* (**Extended Data Fig. 4**). The potency and number of TLR-7/8a linked to each CM conjugate also impacted immunogenicity (**Extended Data Fig. 5**). Additionally, CM conjugates with net positive charge were more potent *in vivo* as compared with those bearing net negative charge (**Extended Data Fig. 6**). Collectively, these data led to an optimal SNP-7/8a formulation based on CM conjugates with net positive charge, comprising cathepsin degradable linkers and 3 TLR-7/8a.

A manufacturing process was developed to enable scalability and rapid per-patient synthesis of SNP-7/8a, which is important for a PCV (**Extended Data Fig. 7**). A simple, copper-free "click chemistry" reaction[46] was used to rapidly link personalized charge-modified peptide neoantigens produced by automated solid-phase synthesis to the pre-built hydrophobic block (oligo-7/8a). The resulting CM conjugates are chemically defined single molecules, which allows for simple release testing, and can be sterile filtered without significant material loss. Addition of aqueous buffer results in the CM conjugates immediately self-assembling to nanoparticles that are stable at room temperature for over 100 hours (**Extended Data Fig. 7**).

Formulation consistency of SNP-7/8a as a PCV

A major challenge for peptide-based PCVs is ensuring formulation consistency given the broad range of neoantigen physicochemical properties. Therefore, to assess the ability of SNP-7/8a to ensure formulation consistency with heterogeneous peptide neoantigens that may be included in PCVs, we first computed the charge and hydropathy frequency distribution of all 25 amino acid peptides (25-mers) that can be generated from each possible single missense mutation in canonical transcripts from the human genome (n = 72.6M mutant 25-mers). About 98% of mutant 25-mers have a charge between –6 to +6 (at pH 7.4) and a grand average of hydropathy (GRAVY) between –2 and +2 (**Fig. 3a**,**b**), which is consistent with the range of properties observed for mouse tumor cell line derived neoantigens (**Extended Data Fig. 8**). To validate the tolerance of SNP-7/8a for delivering neoantigens at the extremes of charge and hydropathy, 9 different mouse neoantigens with a range of underlying charge (–6 to +6) and GRAVY (–2 to +2) were produced as CM conjugates with net positive charge, and all formed stable nanoparticles (**Fig. 3c**).

As PCVs may require multiple predicted neoantigens to be formulated together to maximize T cell breadth, we evaluated the tolerance of SNP-7/8a to formulate multiple CM conjugates with a variety of underlying properties. The SNP-7/8a platform provided consistent particle size, between ~20–50 nm, when the formulation comprised between 5 to 20 different CM conjugates in each particle (**Extended Data Fig. 9a,b**). Interestingly, CM conjugates prone to form aggregates when formulated individually formed stable nanoparticles when formulated together with multiple different CM conjugates (**Extended Data Fig. 9b**).

SNP-7/8a provides improved formulation consistency and immunogenicity

To benchmark immune responses induced by SNP-7/8a against other PCV formulations, 7 MC38-derived neoantigens known to bind MHC-I (Aatf, Adpgk, Cpne1, Dpagt, Irgq, Med12, and Reps1)[12] were evaluated. Each of the neoantigens were formulated either as native LPs admixed with adjuvant (*i.e.*, polyICLC + anti-CD40); as a conjugate vaccine based on LPs linked to a hydrophobic molecule that form microparticles/aggregates (MP-7/8a), which is similar to current conjugate vaccine approaches that do not include a charge modifying group[29-31]; or as CM conjugates of the LPs, which self-assemble into nanoparticles (SNP-7/8a).

The native LPs showed formulation heterogeneity, with 3 out of 7 LPs (Adpgk, Dpagt, and Reps1) forming aggregates, and the remaining 4 occurring as water soluble molecules (**Fig. 4a**). As designed, all LP neoantigens as MP-7/8a and SNP-7/8a assembled into microparticles/aggregates and nanoparticle micelles, respectively. Consistent with the prior report[12], the native LP formulations administered with polyICLC and anti-CD40 induced CD8 responses against 3 of the 7 neoantigens (Adpgk, Dpagt, and Reps1; **Fig 4b**), each of which were particulate, corroborating our prior findings that peptide physical form is a key determinant of immunogenicity (**Fig. 1b**–**g**). Notably, all 7 neoantigens induced high magnitude CD8 T cell

responses when delivered as SNP-7/8a (**Fig. 4b**). Moreover, three of these responses were associated with anti-tumor activity (**Extended Data Fig. 10a**).

Though both conjugate vaccines provided increased breadth of CD8 T cell responses as compared with native LPs admixed with adjuvant (*e.g.*, responses against Cpne1; **Fig. 4b,c**), the nanoparticle micelles (SNP-7/8a) based on CM conjugates induced higher magnitude CD8 T cell responses compared with the microparticle/aggregate formulations (MP-7/8a) based on conjugates without charge modification (**Fig. 4c**). These results suggest that the charge-modifying group may be an important design feature for not only improving formulation characteristics (*i.e.*, preventing aggregation) but also for enhancing the immunogenicity of conjugate vaccines.

SNP-7/8a induces comparable CD8 T cell responses with short and long peptides

Immunization with LPs admixed with adjuvants has been shown to lead to increased magnitude and quality of CD8 T cell responses as compared with the use of Mins[39], possibly due to the requirement of LPs to be processed by professional APCs[47]. However, the impact that peptide length has on the efficiency for inducing CD8 T cell immunity when peptide delivery is controlled with particle carriers is less well established. Therefore, we evaluated T cell responses induced by Min and LP versions of 7 neoantigens as SNP-7/8a. Notably, both Min and LP versions elicited comparable CD8 T cell responses that were of high magnitude (**Fig. 4d**). As expected, only the LPs elicited CD4 T cell responses (**Extended Data Fig. 10b**), likely because the Mins are too short to encode an MHC-II epitope that is contained within some LPs (*e.g.*, Irgq). These results show that both Min and LPs delivered in a particle format can be used to induce CD8 T cells but that LPs may be preferred based on their ability to also elicit CD4 T cells.

SNP-7/8a enhances antigen uptake by lymph node APCs

The physical form of the peptide neoantigen had a major impact on lymph node localization and uptake by antigen presenting cells (APCs). While soluble neoantigen admixed with adjuvant was low to undetectable in draining lymph nodes (**Fig. 5a**) and showed limited uptake by APCs (**Fig. 5b**), both nanoparticle (SNP-7/8a) and microparticle (MP-7/8a) carriers of neoantigens showed substantially higher lymph node accumulation and uptake by APCs. Notably, all formulations induced comparable magnitude and kinetics of innate immune activation in lymph nodes (*i.e.*, IL-12 production; **Fig. 5c**), but CD8 T cell responses were only observed when the peptide neoantigen was delivered in a particle form (**Fig. 5d**).

Comparison of SNP-7/8a (based on CM conjugates) with MP-7/8a (based on peptide antigens linked directly to hydrophobic molecules without charge modification) allowed for the evaluation of how the introduction of the charge-modifying group impacted trafficking and uptake by APCs. Notably, MP-7/8a had lower accumulation in lymph nodes (**Fig. 5a**), lower uptake in APCs (**Fig. 5b**), and induced lower magnitude CD8 T cell responses (**Fig. 5c**) as compared to SNP-7/8a. Together, these data suggest that a critical role of the charge-modifying group is to induce conjugate self-assembly into small (~ 20–50 nm) particles that more efficiently traffic to lymph nodes than conjugates without charge modification, which often assemble into microparticles or aggregates (*i.e.*, MP-7/8a) that form injection site depots.

We next investigated whether differences in lymph node kinetics and APC uptake could account for differences in immunogenicity between native LP neoantigens, Cpne1 and Adpgk, that are soluble and particulate, respectively. The soluble LP neoantigen, Cpne1, was undetectable in draining lymph nodes and exhibited limited uptake by APCs (**Fig. 5e**,**f**). By contrast, the particulate LP neoantigen, Adpgk, showed significantly higher lymph node

accumulation and uptake by APCs (**Fig. 5e**,**f**). While both the soluble and particulate LPs admixed with polyICLC induced comparable levels of innate immune activation (**Fig. 5g**), only the particulate LP led to neoantigen-specific CD8 T cell responses (**Fig. 5h**). These data substantiate that the physical form of the peptide neoantigen, and not any deficiency of the adjuvant (*i.e.*, polyICLC), likely accounts for limited CD8 T cell responses by soluble LPs used in PCVs.

SNP-7/8a increases the breadth of neoantigen-specific CD8 T cell immunity

A correlation between predicted MHC-I binding affinity and immunogenicity is not easily discerned from published data using PCVs based on LP + adjuvant (*i.e.*, polyIC) or RNA (**Fig. 6a**)[13]. However, after controlling for the physical format of 179 peptide-based predicted neoantigens from 3 tumor cell lines in particles co-delivering TLR-7/8a, we observed a strong correlation between predicted MHC-I binding and CD8 T cell responses (**Fig. 6b**). Approximately 50% of epitopes with high predicted binding affinity (IEDB Consensus score < 0.5) led to a CD8 T cell response (**Fig. 6b**). This high efficiency for generating CD8 T cells also allowed for an assessment of the performance of different binding algorithms (see: **Online Methods**) for predicting immunogenicity (**Fig. 6c**). Amongst these, the IEDB Consensus algorithm had the highest predictive value (ROC AUC = 0.83).

Therapeutic vaccination with SNP-7/8a enhances tumor regression

To determine if the improved efficiency of SNP-7/8a could lead to a greater breadth of CD8 T cell responses that mediate tumor clearance *in vivo*, we first screened 24 predicted neoantigens from the B16-F10 tumor cell line (**Extended Data Fig. 11a**) as LPs delivered on SNP-7/8a for the capacity to elicit CD8 T cell responses. Among the 24 predicted neoantigens, 10 induced CD8 T cell responses (**Extended Data Fig. 11b** and **Extended Data Table 1**), of

which 9 or 8 were previously reported to be non-immunogenic using LP + polyIC or RNA, respectively[13]. SNP-7/8a induced CD4 T cell responses against 10 of the 24 LP neoantigens (**Extended Data Table 2**), whereas immunization with LP + polyIC or RNA induced CD4 responses against 9 or 7 of the screened epitopes, respectively.

We then assessed whether 4 of the neoantigens that induced a CD8 T cell response but no significant CD4 T cell response (*i.e.*, M01, M07, M21, and M39) could limit tumor growth when used as a therapeutic vaccine administered intravenously (IV) and combined with a CPI. This therapeutic regimen was based on the observation that vaccines combined with CPIs (*e.g.*, anti-PD-1, anti-PD-L1, or anti-CTLA-4) improve tumor control as compared with either vaccines or CPIs alone[48] and that administration of peptide- and RNA-based vaccines by the IV route of administration can enhance therapeutic efficacy[29,49]. Indeed, a potential advantage of conjugate vaccines, such as SNP-7/8a, is that peptide antigens can be covalently attached to adjuvants (*e.g.*, TLR-7/8a) to ensure that both are co-delivered to APCs, which may be needed for optimal T cell priming[33,34], following vaccination by any route of administration.

Vaccination with SNP-7/8a delivering either the neoantigens M07, M21, or M39 led to improved control of tumor growth (**Fig. 6d**,**e** and **Extended Data Fig. 11c**). To further substantiate that CD8 T cells were responsible for mediating the anti-tumor effect, M39-vaccinated animals were treated with a CD8 depleting antibody and the animals showed no control of tumor growth (**Extended Data Fig. 11d**). Importantly, these results show that the improved efficiency of the SNP-7/8a vaccine platform leads to a greater number of CD8 T cell specificities capable of mediating tumor control.

Finally, to assess the broader potential of the SNP-7/8a platform as a therapeutic cancer vaccine, we evaluated the ability of SNP-7/8a delivering different tumor antigens, including self-

antigens (Trp1 for B16-F10; **Extended Data Fig. 11c**), neoantigens (Adpgk for MC38; **Fig. 6f,g**), and viral antigens (E7 for TC-1; **Extended Data Fig. 12**), to mediate clearance of tumor cells. In each case, therapeutic vaccination with SNP-7/8a led to enhanced control of established tumors. These results highlight the broad therapeutic potential of SNP-7/8a to induce T cells for targeting diverse tumor antigens.

DISCUSSION

Herein we show that peptide antigen physical form is a major determinant of CD8 T cell induction by peptide-based vaccines. Soluble peptides, which may be preferentially selected in clinical-grade peptide vaccines because of their ease of manufacturing[14], fail to accumulate in APCs in lymphoid tissue and prime CD8 T cell responses. Consistent with these observations, prior studies have shown that attachment of fatty acids to peptide antigens results in amphiphilic conjugates that lead to higher magnitude CD8 T cell responses as compared with hydrophilic native peptide antigens mixed with polyIC[29]. The data presented here extend these findings by showing that – across multiple different antigens and adjuvants (*i.e.,* polyICLC, CpG, and TLR-7/8a) – increasing the amphiphilic/hydrophobic character of peptide antigens leads to particle formation that is associated with enhanced CD8 T cell responses. These results have important translational implications and suggest that peptide antigens used in cancer vaccines should be rendered particulate to maximize immunogenicity.

Our observation that soluble peptide antigens are more rapidly cleared from the injection site and draining lymph nodes than particulate antigens may in part account for enhanced CD8 T cell responses by particulate antigens. Indeed, soluble TLRa that freely disperse from vaccine injection sites and exhibit rapid clearance were shown to be less effective for inducing T cells than particulate adjuvants that are retained within draining lymphatics after injection[42,50]. Taken together, these findings suggest that a key role of particles is to limit biodistribution and concentrate vaccines (antigen and adjuvants) in lymphoid organs. Though, improved stability against lysosomal proteolysis[51] and enhanced efficiency of capture by lymph node DCs[52] may be additional mechanisms that account for improved CD8 T cell immunogenicity by particle antigens. Indeed, additional studies will be needed to provide a greater understanding of how

particle composition, size, charge and shape, as well as adjuvant combinations impact T cell responses with particle formulations of neoantigens.

A broad variety of particle vaccine technologies have been developed to enhance the immunogenicity of protein- and peptide-based cancer vaccines[48,53-55]. However, such approaches may be limited by inconsistent material loading and/or formulation variability arising from differences in antigen properties, which are compounded by the need to sterile filter particle formulations using <0.2 μm pore membranes that can be clogged by heterogeneous particle formulations and can result in material loss[56]. These limitations of current particle vaccine technologies can complicate manufacturing and product release, particularly for a personalized, on-demand therapy. In contrast, the charge-modified conjugates described herein are chemically-defined single molecules (100% material loading) that allow for facile sterile filtration without material loss and ensure consistent formulations through a controlled nanoparticle self-assembly process.

While other conjugate vaccine technologies have been shown to be effective for inducing anticancer T cell immunity[28,29,32], a major limitation is their propensity to form aggregates that can complicate manufacturing and lead to injection-site depots that can cause T cell exhaustion[57]. Herein, we introduced a charge-modifying group to the N-terminus of peptide antigens as a novel conjugate vaccine feature that i) improves the solubility of hydrophobic peptide antigens during synthesis and purification and ii) provides a driving force for inducing uniformly-sized nanoparticles of a size range (*i.e.*, 20–50 nm) that is reported to be optimal for targeting DCs that promote T cell immunity[58,59]. Importantly, SNP-7/8a based on CM conjugates enhanced uptake by APCs and led to superior CD8 T cell induction over conjugates without charge modification.

An additional notable finding was that an absolute net charge of >5 was needed to ensure nanoparticle micellization using CM conjugates based on a variety of different antigens, hydrophobic molecules (cholesterol, fatty acids, lipids and oligopeptides) and agonists (TLRa, NLRa and STINGa). These findings were validated using a machine learning model and suggest that the dependency of high net charge on nanoparticle micellization may be generalizable to other conjugate vaccines. Though, additional studies will be needed to determine how net charge impacts the size and stability of other particle vaccine technologies, including micelle-forming polymers that can be neutral yet still form stable micelles[60,61].

Though advances in genomic sequencing technologies and *in silico* MHC-I binding prediction algorithms have enabled rapid identification and selection of neoantigens to include in PCVs[62,63], many of the neoantigens included in peptide-based PCVs to-date have failed to induce *de novo* CD8 T cell responses[13,14], possibly due to differences in neoantigen physical form. In contrast, the CM conjugates described herein enabled the evaluation of the relationship between different MHC-I binding affinity prediction algorithms and *in vivo* CD8 T cell immunogenicity without confounding due to differences in neoantigen physical form. Consistent with recent reports that many neoantigen-specific CD8 T cells identified in patients have high predicted MHC-I binding affinity[10,64,65], we observed a robust correlation between MHC-I binding affinity and immunogenicity ($P < 0.0001$) and determined that the IEDB Consensus algorithm had the highest predictive value of the algorithms tested (ROC AUC = 0.83). Our results indicate that efficient PCVs that control for the widely-variable underlying neoantigen properties may be needed to produce reliable data sets for training the next generation of prediction algorithms.

In benchmarking the activity of SNP-7/8a based on CM conjugates, all 7 MC38 neoantigens with confirmed MHC-I binding induced high magnitude CD8 T cell responses,

while only 3 were immunogenic with LP + polyICLC. In a larger screen of predicted neoantigens delivered on SNP-7/8a, we observed CD8 T cell responses against ~50% of predicted neoantigens with high MHC-I binding affinity (IEDB Consensus score < 0.5), which is about a 5-fold improvement over published rates (~10%) using PCVs based on LP + polyIC or RNA[13]. This improved efficiency for inducing CD8 T cell responses may allow for the targeting of a broader repertoire of neoantigens in a given patient and the treatment of tumors with lower mutational burden, where neoantigen targets are more limited[16].

The preference for using LPs in cancer vaccines is based in part on the observation that LPs require processing by professional APCs while Mins can be presented by other cells that may result in the induction of tolerance[47,66]. Here, we show that both Min and LP neoantigens induced comparable magnitude and breadth of CD8 T cell responses when delivered as SNP-7/8a. A possible explanation is that covalent attachment of Mins to particles (*e.g.*, SNP-7/8a) may endow particulate Mins with a processing requirement that is otherwise a benefit unique to LPs. Indeed, use of Mins in a variety of other particle[54] and conjugate[54,67] vaccine technologies have been shown to induce robust CD8 T cell immunity. However, since longer peptides may also contain CD4 T cell epitopes[13,14], LPs may be preferred over Mins in PCVs.

Our rationale for using the IV route of administration for therapeutic vaccination was based on recent observations that systemic delivery provides superior efficacy as compared with other commons routes of administration[49,67]. Though, the success of PCVs given IV will likely require the combination of antigen and adjuvant in the same particle (*e.g.*, SNP-7/8a) to ensure that both components are co-delivered to APCs while also limiting non-specific inflammation resulting from systemic distribution of adjuvant without antigen.

Finally, a major focus for advancing PCVs, such as SNP-7/8a, will be on identifying the optimal combination with complementary immunotherapies (*e.g.*, IL-2, tumor-specific antibodies, and CPIs)[68] and chemotherapeutics[69] that promote efficient tumor killing while maintaining acceptable safety profiles.

Altogether, the results presented herein show how a peptide-based PCV can be systematically optimized to enhance the magnitude and breadth of neoantigen-specific T cell responses while addressing manufacturing challenges of a fully personalized therapy. These results have implications for the design and implementation of PCVs, including the refinement of algorithms that prioritize predicted neoantigens for inclusion in PCVs.

REFERENCES

1 Segal, N. H. *et al.* Epitope landscape in breast and colorectal cancer. *Cancer Res* **68**, 889-892, doi:10.1158/0008-5472.CAN-07-3095 (2008).

2 Lennerz, V. *et al.* The response of autologous T cells to a human melanoma is dominated by mutated neoantigens. *Proc Natl Acad Sci U S A* **102**, 16013-16018, doi:10.1073/pnas.0500090102 (2005).

3 Tran, E. *et al.* Cancer immunotherapy based on mutation-specific CD4+ T cells in a patient with epithelial cancer. *Science* **344**, 641-645, doi:10.1126/science.1251102 (2014).

4 Tran, E. *et al.* T-Cell Transfer Therapy Targeting Mutant KRAS in Cancer. *N Engl J Med* **375**, 2255-2262, doi:10.1056/NEJMoa1609279 (2016).

5 Snyder, A. *et al.* Genetic basis for clinical response to CTLA-4 blockade in melanoma. *N Engl J Med* **371**, 2189-2199, doi:10.1056/NEJMoa1406498 (2014).

6 Rizvi, N. A. *et al.* Cancer immunology. Mutational landscape determines sensitivity to PD-1 blockade in non-small cell lung cancer. *Science* **348**, 124-128, doi:10.1126/science.aaa1348 (2015).

7 Rosenberg, J. E. *et al.* Atezolizumab in patients with locally advanced and metastatic urothelial carcinoma who have progressed following treatment with platinum-based chemotherapy: a single-arm, multicentre, phase 2 trial. *Lancet* **387**, 1909-1920, doi:10.1016/S0140-6736(16)00561-4 (2016).

8 Castle, J. C. *et al.* Exploiting the mutanome for tumor vaccination. *Cancer Res* **72**, 1081-1091, doi:10.1158/0008-5472.CAN-11-3722 (2012).

9 Yarchoan, M., Johnson, B. A., 3rd, Lutz, E. R., Laheru, D. A. & Jaffee, E. M. Targeting neoantigens to augment antitumour immunity. *Nat Rev Cancer* **17**, 209-222, doi:10.1038/nrc.2016.154 (2017).

10 Sahin, U. & Tureci, O. Personalized vaccines for cancer immunotherapy. *Science* **359**, 1355-1360, doi:10.1126/science.aar7112 (2018).

11 Hu, Z., Ott, P. A. & Wu, C. J. Towards personalized, tumour-specific, therapeutic vaccines for cancer. *Nat Rev Immunol* **18**, 168-182, doi:10.1038/nri.2017.131 (2018).

12 Yadav, M. *et al.* Predicting immunogenic tumour mutations by combining mass spectrometry and exome sequencing. *Nature* **515**, 572-576, doi:10.1038/nature14001 (2014).

13 Kreiter, S. *et al.* Mutant MHC class II epitopes drive therapeutic immune responses to cancer. *Nature* **520**, 692-696, doi:10.1038/nature14426 (2015).

14 Ott, P. A. *et al.* An immunogenic personal neoantigen vaccine for patients with melanoma. *Nature* **547**, 217-221, doi:10.1038/nature22991 (2017).

15 Sahin, U. *et al.* Personalized RNA mutanome vaccines mobilize poly-specific therapeutic immunity against cancer. *Nature* **547**, 222-226, doi:10.1038/nature23003 (2017).

16 Schumacher, T. N. & Schreiber, R. D. Neoantigens in cancer immunotherapy. *Science* **348**, 69-74, doi:10.1126/science.aaa4971 (2015).

17 Dubensky, T. W., Jr. & Reed, S. G. Adjuvants for cancer vaccines. *Semin Immunol* **22**, 155-161, doi:S1044-5323(10)00048-5 [pii]
10.1016/j.smim.2010.04.007 (2010).

18 Irvine, D. Material aid for vaccines. *Nat Mater* **17**, 472-473, doi:10.1038/s41563-018-0089-2 (2018).
19 Zhu, G., Zhang, F., Ni, Q., Niu, G. & Chen, X. Efficient Nanovaccine Delivery in Cancer Immunotherapy. *ACS Nano* **11**, 2387-2392, doi:10.1021/acsnano.7b00978 (2017).
20 Fan, Y. & Moon, J. J. Nanoparticle Drug Delivery Systems Designed to Improve Cancer Vaccines and Immunotherapy. *Vaccines (Basel)* **3**, 662-685, doi:10.3390/vaccines3030662 (2015).
21 Fontana, F., Liu, D., Hirvonen, J. & Santos, H. A. Delivery of therapeutics with nanoparticles: what's new in cancer immunotherapy? *Wiley Interdiscip Rev Nanomed Nanobiotechnol* **9**, doi:10.1002/wnan.1421 (2017).
22 Kim, H. *et al.* Polymeric nanoparticles encapsulating novel TLR7/8 agonists as immunostimulatory adjuvants for enhanced cancer immunotherapy. *Biomaterials* **164**, 38-53, doi:10.1016/j.biomaterials.2018.02.034 (2018).
23 Ilyinskii, P. O. *et al.* Adjuvant-carrying synthetic vaccine particles augment the immune response to encapsulated antigen and exhibit strong local immune activation without inducing systemic cytokine release. *Vaccine* **32**, 2882-2895, doi:10.1016/j.vaccine.2014.02.027 (2014).
24 Varypataki, E. M. *et al.* Synthetic long peptide-based vaccine formulations for induction of cell mediated immunity: A comparative study of cationic liposomes and PLGA nanoparticles. *J Control Release* **226**, 98-106, doi:10.1016/j.jconrel.2016.02.018 (2016).
25 Scott, E. A. *et al.* Dendritic cell activation and T cell priming with adjuvant- and antigen-loaded oxidation-sensitive polymersomes. *Biomaterials* **33**, 6211-6219, doi:10.1016/j.biomaterials.2012.04.060 (2012).
26 Aucouturier, J., Dupuis, L., Deville, S., Ascarateil, S. & Ganne, V. Montanide ISA 720 and 51: a new generation of water in oil emulsions as adjuvants for human vaccines. *Expert Rev Vaccines* **1**, 111-118, doi:10.1586/14760584.1.1.111 (2002).
27 Fox, C. B. & Haensler, J. An update on safety and immunogenicity of vaccines containing emulsion-based adjuvants. *Expert Rev Vaccines* **12**, 747-758, doi:10.1586/14760584.2013.811188 (2013).
28 Liu, H. *et al.* Structure-based programming of lymph-node targeting in molecular vaccines. *Nature* **507**, 519-522, doi:10.1038/nature12978 (2014).
29 Cho, H. I., Barrios, K., Lee, Y. R., Linowski, A. K. & Celis, E. BiVax: a peptide/poly-IC subunit vaccine that mimics an acute infection elicits vast and effective anti-tumor CD8 T-cell responses. *Cancer Immunol Immunother* **62**, 787-799, doi:10.1007/s00262-012-1382-6 (2013).
30 Ignacio, B. J., Albin, T. J., Esser-Kahn, A. P. & Verdoes, M. Toll-like Receptor Agonist Conjugation: A Chemical Perspective. *Bioconjug Chem* **29**, 587-603, doi:10.1021/acs.bioconjchem.7b00808 (2018).
31 Zom, G. G. *et al.* Efficient induction of antitumor immunity by synthetic toll-like receptor ligand-peptide conjugates. *Cancer Immunol Res* **2**, 756-764, doi:10.1158/2326-6066.CIR-13-0223 (2014).
32 Zhu, G. *et al.* Albumin/vaccine nanocomplexes that assemble in vivo for combination cancer immunotherapy. *Nat Commun* **8**, 1954, doi:10.1038/s41467-017-02191-y (2017).

33 Blander, J. M. & Medzhitov, R. Toll-dependent selection of microbial antigens for presentation by dendritic cells. *Nature* **440**, 808-812, doi:nature04596 [pii] 10.1038/nature04596 (2006).
34 Nair-Gupta, P. *et al.* TLR signals induce phagosomal MHC-I delivery from the endosomal recycling compartment to allow cross-presentation. *Cell* **158**, 506-521, doi:10.1016/j.cell.2014.04.054 (2014).
35 Hailemichael, Y. & Overwijk, W. W. Peptide-based anticancer vaccines: The making and unmaking of a T-cell graveyard. *Oncoimmunology* **2**, e24743, doi:10.4161/onci.24743 (2013).
36 Gnjatic, S. & Bhardwaj, N. Antigen depots: T cell traps? *Nat Med* **19**, 397-398, doi:10.1038/nm.3113 (2013).
37 Salerno, E. P. *et al.* Activation, dysfunction and retention of T cells in vaccine sites after injection of incomplete Freund's adjuvant, with or without peptide. *Cancer Immunol Immunother* **62**, 1149-1159, doi:10.1007/s00262-013-1435-5 (2013).
38 Kenter, G. G. *et al.* Vaccination against HPV-16 oncoproteins for vulvar intraepithelial neoplasia. *N Engl J Med* **361**, 1838-1847, doi:10.1056/NEJMoa0810097 (2009).
39 Melief, C. J. & van der Burg, S. H. Immunotherapy of established (pre)malignant disease by synthetic long peptide vaccines. *Nat Rev Cancer* **8**, 351-360, doi:10.1038/nrc2373 (2008).
40 Melief, C. *Peptide-Based Therapeutic Cancer Vaccines*. (2018).
41 Cavalli, S., Albericio, F. & Kros, A. Amphiphilic peptides and their cross-disciplinary role as building blocks for nanoscience. *Chem Soc Rev* **39**, 241-263, doi:10.1039/b906701a (2010).
42 Lynn, G. M. *et al.* In vivo characterization of the physicochemical properties of polymer-linked TLR agonists that enhance vaccine immunogenicity. *Nat Biotechnol* **33**, 1201-1210, doi:10.1038/nbt.3371 (2015).
43 Liaw, A. & Wiener, M. Classification and Regression by randomForest. *R News* **2**, 18-22, doi:citeulike-article-id:1121494 (2002).
44 Choe, Y. *et al.* Substrate profiling of cysteine proteases using a combinatorial peptide library identifies functionally unique specificities. *J Biol Chem* **281**, 12824-12832, doi:10.1074/jbc.M513331200 (2006).
45 Kloetzel, P. M. Antigen processing by the proteasome. *Nat Rev Mol Cell Biol* **2**, 179-187, doi:10.1038/35056572 (2001).
46 Jewett, J. C. & Bertozzi, C. R. Cu-free click cycloaddition reactions in chemical biology. *Chem Soc Rev* **39**, 1272-1279 (2010).
47 Bijker, M. S. *et al.* CD8+ CTL priming by exact peptide epitopes in incomplete Freund's adjuvant induces a vanishing CTL response, whereas long peptides induce sustained CTL reactivity. *J Immunol* **179**, 5033-5040 (2007).
48 Luo, M. *et al.* A STING-activating nanovaccine for cancer immunotherapy. *Nat Nanotechnol* **12**, 648-654, doi:10.1038/nnano.2017.52 (2017).
49 Kranz, L. M. *et al.* Systemic RNA delivery to dendritic cells exploits antiviral defence for cancer immunotherapy. *Nature* **534**, 396-401, doi:10.1038/nature18300 (2016).
50 Wu, T. Y. *et al.* Rational design of small molecules as vaccine adjuvants. *Sci Transl Med* **6**, 263ra160, doi:10.1126/scitranslmed.3009980 (2014).

51 Delamarre, L., Pack, M., Chang, H., Mellman, I. & Trombetta, E. S. Differential lysosomal proteolysis in antigen-presenting cells determines antigen fate. *Science* **307**, 1630-1634, doi:10.1126/science.1108003 (2005).
52 Gerner, M. Y., Torabi-Parizi, P. & Germain, R. N. Strategically localized dendritic cells promote rapid T cell responses to lymph-borne particulate antigens. *Immunity* **42**, 172-185, doi:10.1016/j.immuni.2014.12.024 (2015).
53 Kim, J. *et al.* Injectable, spontaneously assembling, inorganic scaffolds modulate immune cells in vivo and increase vaccine efficacy. *Nat Biotechnol* **33**, 64-72, doi:10.1038/nbt.3071 (2015).
54 Kuai, R., Ochyl, L. J., Bahjat, K. S., Schwendeman, A. & Moon, J. J. Designer vaccine nanodiscs for personalized cancer immunotherapy. *Nat Mater* **16**, 489-496, doi:10.1038/nmat4822 (2017).
55 Hanson, M. C. *et al.* Nanoparticulate STING agonists are potent lymph node-targeted vaccine adjuvants. *J Clin Invest* **125**, 2532-2546, doi:10.1172/JCI79915 (2015).
56 Wendorf, J. *et al.* A practical approach to the use of nanoparticles for vaccine delivery. *J Pharm Sci* **95**, 2738-2750, doi:10.1002/jps.20728 (2006).
57 Hailemichael, Y. *et al.* Persistent antigen at vaccination sites induces tumor-specific CD8(+) T cell sequestration, dysfunction and deletion. *Nat Med* **19**, 465-472, doi:10.1038/nm.3105 (2013).
58 Bachmann, M. F. & Jennings, G. T. Vaccine delivery: a matter of size, geometry, kinetics and molecular patterns. *Nat Rev Immunol* **10**, 787-796, doi:10.1038/nri2868 (2010).
59 Manolova, V. *et al.* Nanoparticles target distinct dendritic cell populations according to their size. *Eur J Immunol* **38**, 1404-1413, doi:10.1002/eji.200737984 (2008).
60 Keller, S. *et al.* Neutral polymer micelle carriers with pH-responsive, endosome-releasing activity modulate antigen trafficking to enhance CD8(+) T cell responses. *J Control Release* **191**, 24-33, doi:10.1016/j.jconrel.2014.03.041 (2014).
61 Sevimli, S., Knight, F. C., Gilchuk, P., Joyce, S. & Wilson, J. T. Fatty Acid-Mimetic Micelles for Dual Delivery of Antigens and Imidazoquinoline Adjuvants. *ACS Biomater Sci Eng* **3**, 179-194, doi:10.1021/acsbiomaterials.6b00408 (2017).
62 Abelin, J. G. *et al.* Mass Spectrometry Profiling of HLA-Associated Peptidomes in Mono-allelic Cells Enables More Accurate Epitope Prediction. *Immunity* **46**, 315-326, doi:10.1016/j.immuni.2017.02.007 (2017).
63 Rubinsteyn, A. *et al.* Computational Pipeline for the PGV-001 Neoantigen Vaccine Trial. *Front Immunol* **8**, 1807, doi:10.3389/fimmu.2017.01807 (2017).
64 Stronen, E. *et al.* Targeting of cancer neoantigens with donor-derived T cell receptor repertoires. *Science* **352**, 1337-1341, doi:10.1126/science.aaf2288 (2016).
65 Tran, E. *et al.* Immunogenicity of somatic mutations in human gastrointestinal cancers. *Science* **350**, 1387-1390, doi:10.1126/science.aad1253 (2015).
66 Bijker, M. S. *et al.* Superior induction of anti-tumor CTL immunity by extended peptide vaccines involves prolonged, DC-focused antigen presentation. *Eur J Immunol* **38**, 1033-1042, doi:10.1002/eji.200737995 (2008).
67 Sultan, H. *et al.* Designing therapeutic cancer vaccines by mimicking viral infections. *Cancer Immunol Immunother* **66**, 203-213, doi:10.1007/s00262-016-1834-5 (2017).

68 Moynihan, K. D. *et al.* Eradication of large established tumors in mice by combination immunotherapy that engages innate and adaptive immune responses. *Nat Med* **22**, 1402-1410, doi:10.1038/nm.4200 (2016).
69 Welters, M. J. *et al.* Vaccination during myeloid cell depletion by cancer chemotherapy fosters robust T cell responses. *Sci Transl Med* **8**, 334ra352, doi:10.1126/scitranslmed.aad8307 (2016).

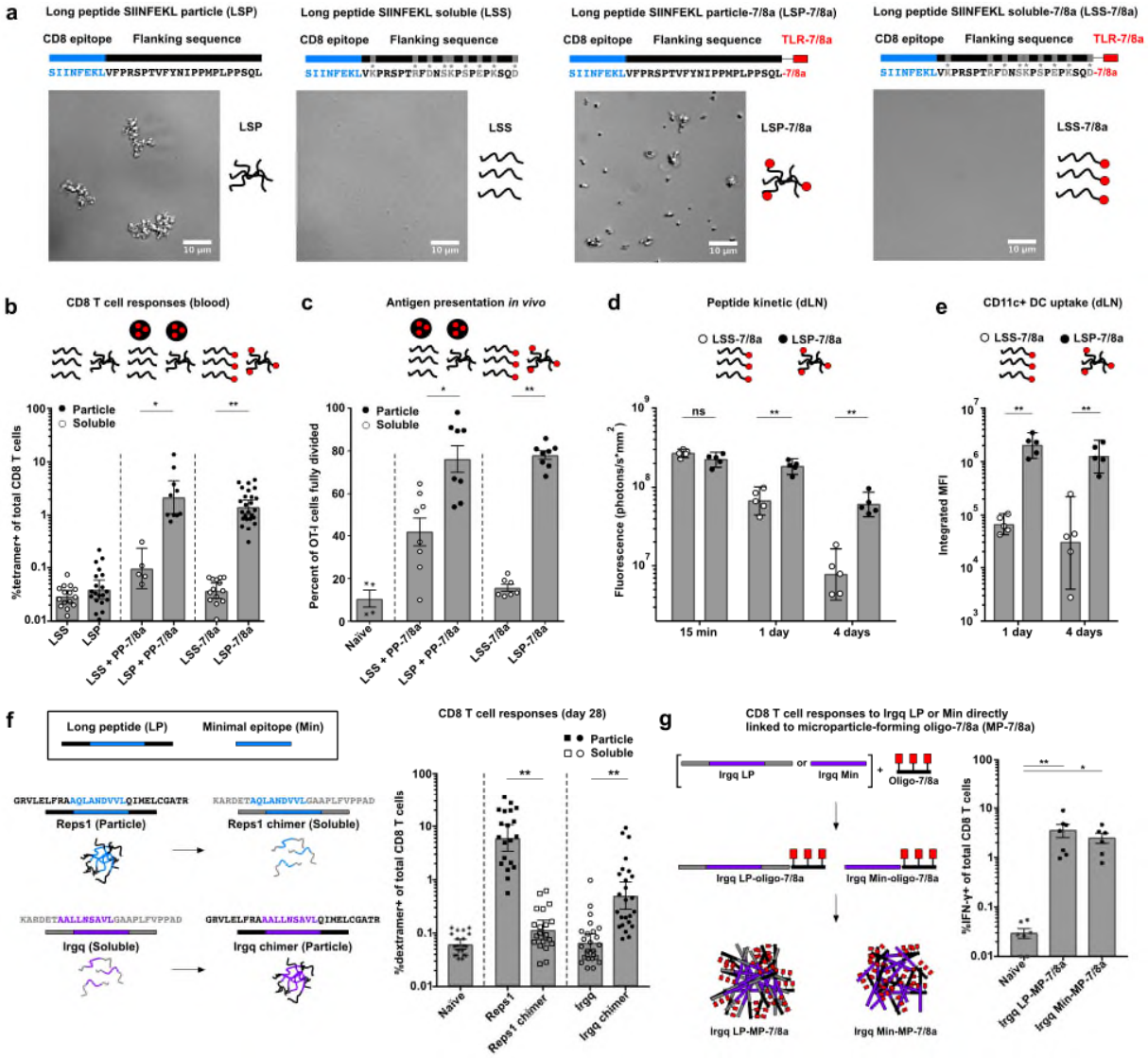

Figure 1: Peptide physical form is a key determinant of CD8 T cell immunogenicity.
(**a**) Schematic and brightfield micrographs of the CD8 T cell epitope from Ovalbumin (SIINFEKL) contained within long peptides (LP) that are either particulate (LSP and LSP-7/8a) or soluble (LSS and LSS-7/8a) in PBS. (**b**) C57BL/6 mice (n = 5–25 per group) were immunized with the specified formulations on days 0 and 14, and CD8 T cell responses were assessed by tetramer staining on day 28. (**c**) C57BL/6 mice (n = 8 per group) were immunized subcutaneously with the specified formulations followed by intravenous adoptive transfer of CFSE-labeled OT-I cells. On day 6, cell division of OT-I cells was assessed by flow cytometry. (**d**,**e**). C57BL/6 mice (n = 5 per group per time point) were immunized subcutaneously in the footpad with AlexaFluor647-labeled LSS-7/8a or LSP-7/8a, and draining lymph nodes (dLN) were assessed for (**d**) total tissue fluorescence and (**e**) vaccine uptake by CD11c+ DCs. (**f**) Native and chimeric forms of Reps1 and Irgq LP neoantigens were admixed with an adjuvant (either PP-7/8a, CpG, or polyICLC) and administered to C57BL/6 mice (n = 10–25 per group) at days 0 and 14. CD8 T cell responses from blood were determined by dextramer staining on day 28, and

responses compiled across all adjuvants are shown. (**g**) C57BL/6 mice (n = 7 per group) were immunized with MP-7/8a containing the LP or Min form of the neoantigen Irgq at days 0 and 14, and CD8 T cell responses were assessed by intracellular cytokine staining on day 28. PP-7/8a is a particle-forming polymer-TLR-7/8a adjuvant. Data on log scale are reported as geometric mean with 95% c.i.; data on linear scale are reported at mean ± s.e.m. Statistical significance was determined using Kruskal-Wallis with Dunn's correction (**b**,**c**,**f**,**g)** or two-way ANOVA with Bonferroni correction (**d**,**e**); ns = not significant, *$P < 0.05$, **$P \leq 0.01$.

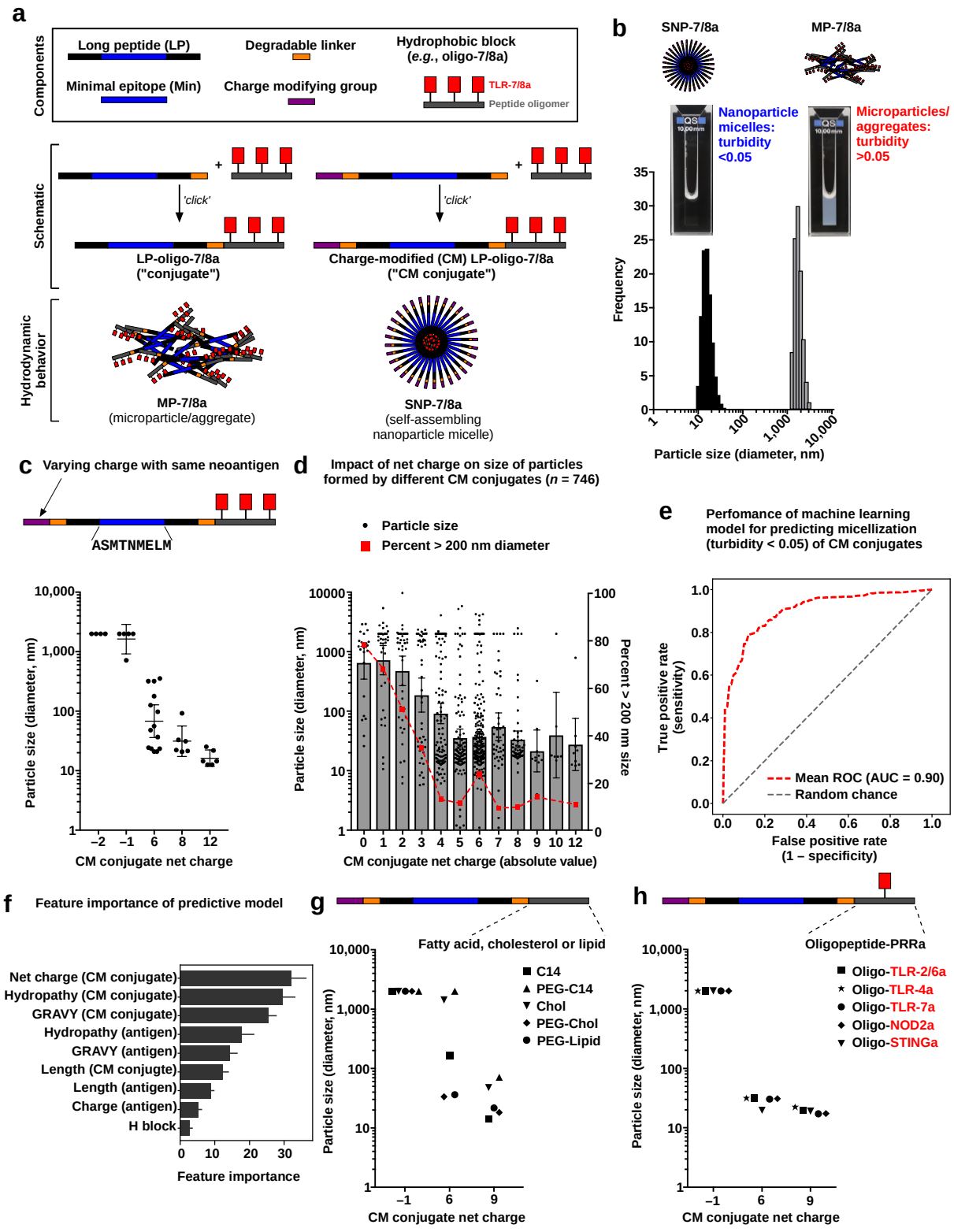

Figure 2: Self-assembling nanoparticles (SNP-7/8a) based on charge-modified peptide-TLR-7/8a conjugates.

(**a**) Schematic of modular components comprising peptide-TLR-7/8a conjugate vaccines and charge-modified (CM) peptide-TLR-7/8a conjugate vaccines that form microparticles/aggregates (MP-7/8a) and self-assembling nanoparticle micelles (SNP-7/8a), respectively. (**b**) Particle size distribution plot for representative SNP-7/8a and MP-7/8a. (**c**) Particle sizes of CM conjugates with various charge modifying groups appended to the same peptide antigen sequence. (**d**) Particle sizes of different CM conjugates (n = 746) with varying net charge (absolute value). (**e**) Receiver operating characteristic (ROC) curves of a random forest machine learning model for predicting SNP-7/8a hydrodynamic behavior for any given CM conjugate composition; mean ROC is the average performance of the models based on a 10-fold cross-validated binary classifier trained on data from **d**. (**f**) The relative importance of different characteristics of CM conjugates on the performance of the ML model from **e**. (**g**) Particle size dependency on net charge of CM conjugates containing various hydrophobic blocks. (**h**) Particle size dependency on net charge of CM conjugates containing hydrophobic blocks based on peptide oligomers linked to various pattern recognition receptor (PRR) agonists. C14 = myristic acid; chol = cholesterol. Data on log scale are reported as geometric mean with 95% c.i.

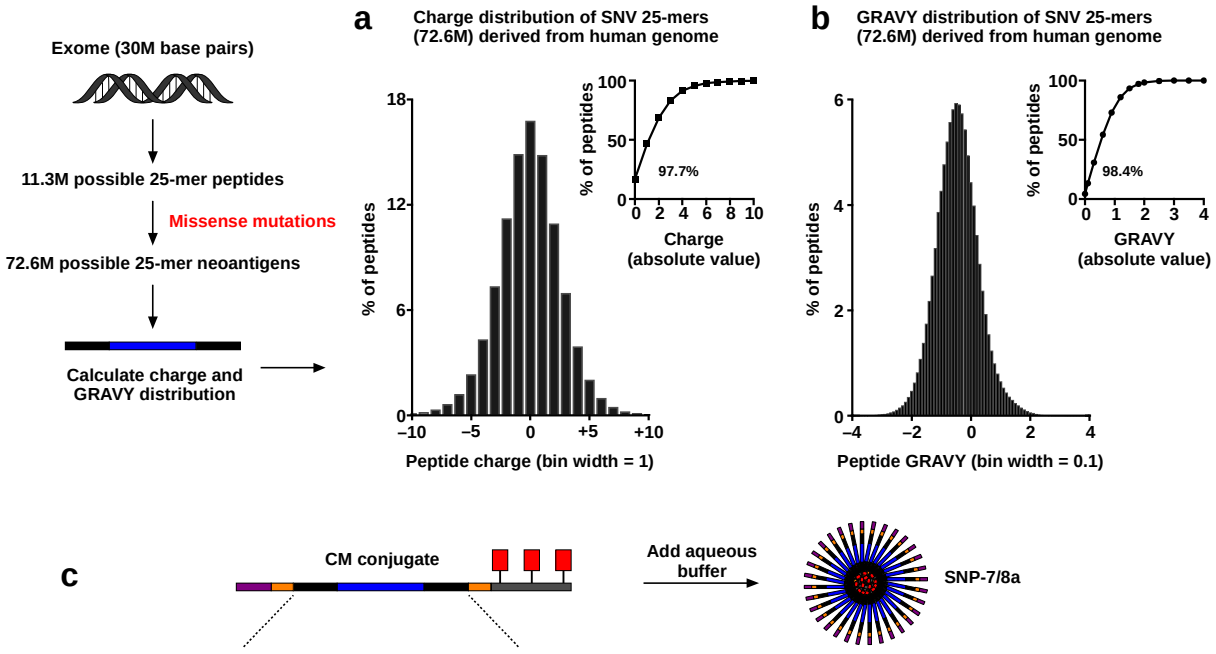

Predicted neoantigen properties			SNP-7/8a properties	
Peptide sequence	Charge	GRAVY	Size (d, nm)	Turbidity
ETLGEISFLLSLDLHFTDGDYSAGD	–6	0.02	18.2	0.04
DDEGDYTCQFTHVENGTNYIVTATR	–4	–0.90	39.4	0.04
GIPVHLELASMTNMELMSSIVHQQVFPT	–2	0.43	32.9	0.04
VVDRNPQFLDPVLAYLMKGLCEKPLAS	0	0.20	17.4	0.04
NIEGIDKLTQLKKPFLVNNKINKIENI	2	–0.47	19.3	0.04
MAAALTFRRLLTLPRAARGFGVQVS	4	0.56	23.6	0.04
GRGHLLGRLAAIVGKQVLLGRKVVVVR	6	0.66	73.7	0.04
QGTDVVIAIFIILAMSFVPASFVVF	–1	2.00	30.3	0.04
LKSSPERNDWEPLDKKVDTRKYRAE	1	–1.91	30.6	0.04

Figure 3: Genome-wide analysis of LP neoantigen charge and hydropathy frequency distribution validates SNP-7/8a as a PCV.
(**a**) Charge and (**b**) hydropathy (GRAVY) frequency distribution of 25 amino acid LPs derived from all possible non-synonymous single nucleotide variant (SNV) missense mutations in canonical protein coding transcripts (*n* = 72.6M mutant 25-mers); inset shows the cumulative proportion of mutant 25-mers with a given range of characteristics (*i.e.*, ~ 98% of possible neoantigen peptides have charge between –6 to +6 and GRAVY between –2 and +2). (**c**) Predicted neoantigens (mouse-derived) with the indicated charge and GRAVY characteristics were synthesized as CM conjugates, and the particle size (diameter, nm) and turbidity (absorbance at 490 nm) of those particles (SNP-7/8a) in PBS, pH 7.4 was assessed. Absorbance at 490 nm > 0.05 indicates aggregation.

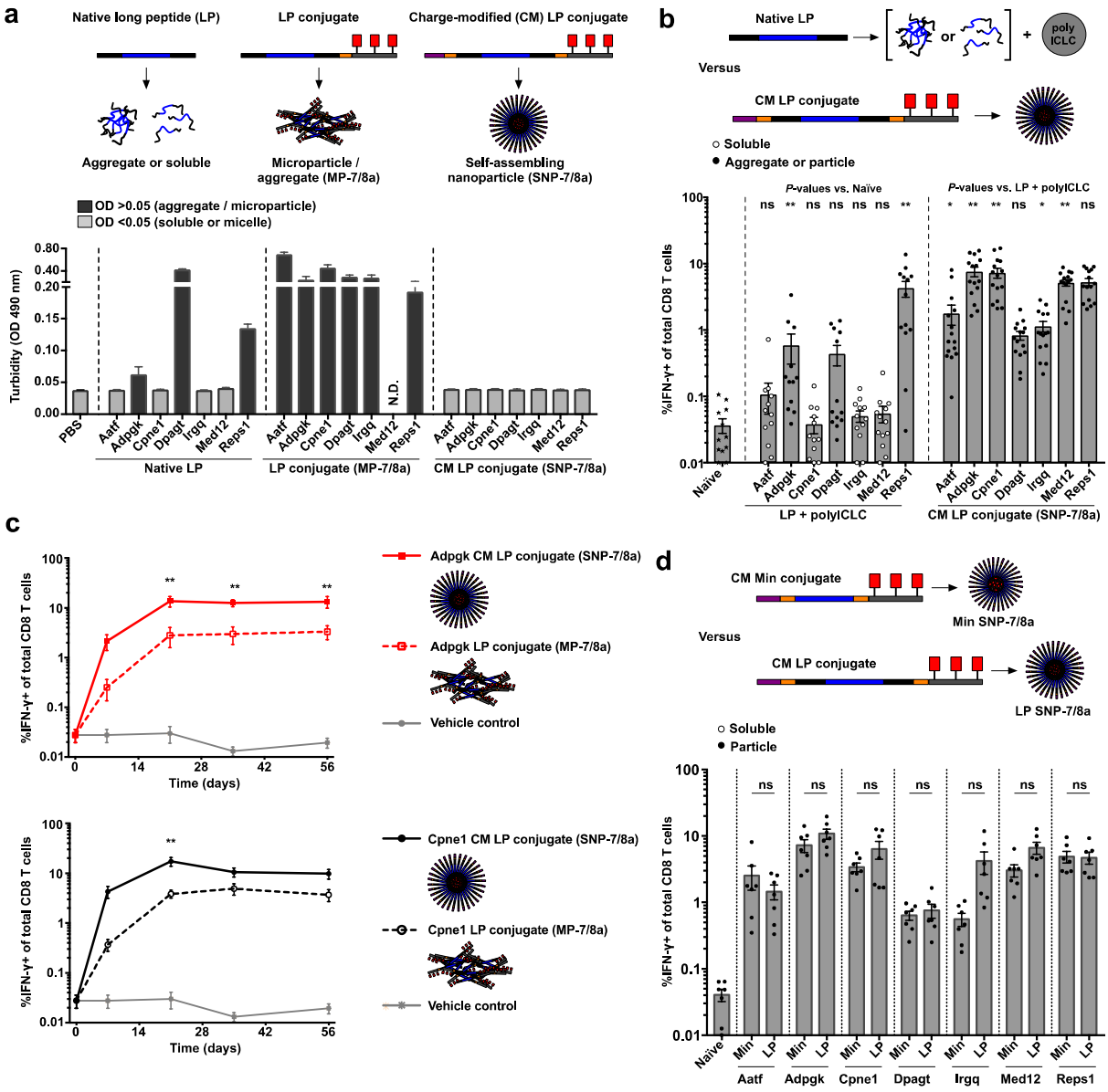

Figure 4: SNP-7/8a improves formulation consistency and immunogenicity over conventional PCV approaches.

(**a**–**d**) Seven MC38 neoantigens known to bind MHC-I (Aatf, Adpgk, Cpne1, Dpagt, Irgq, Med12, and Reps1) were produced as either native LPs; conjugates of oligo-7/8a that form microparticles/aggregates (MP-7/8a); or charge-modified (CM) conjugates of oligo-7/8a that self-assemble to nanoparticles (SNP-7/8a). (**a**) Turbidity of the LP formulations at 0.5 mg/mL in PBS pH 7.4 was assessed by measuring absorbance at 490 nm; absorbance > 0.05 indicates aggregation. (**b**) C57BL/6 mice (n = 13–15 per group) were immunized with native LPs admixed with polyICLC or as SNP-7/8a on days 0 and 14, and CD8 T cell responses were assessed from blood by intracellular cytokine staining on day 28. (**c**) C57BL/6 mice (n = 5 per group) were immunized with either Cpne1 or Adpgk LPs as MP-7/8a or SNP-7/8a on days 0, 14, and 28, and CD8 T cell responses were assessed as in **b** at various time points. (**d**) C57BL/6 mice (n = 5 per

group) were immunized with SNP-7/8a including either the LP or Min forms of different neoantigens on days 0 and 14, and CD8 T cell responses were assessed as in **c**. n.d. = not determined. Data on log scale are reported as geometric mean with 95% c.i.; data on linear scale are reported at mean ± s.e.m. Statistical significance was determined using Kruskal-Wallis with Dunn's correction (**b**,**d**) or two-way ANOVA with Bonferroni correction (**c**); ns = not significant, *$P < 0.05$, **$P \leq 0.01$.

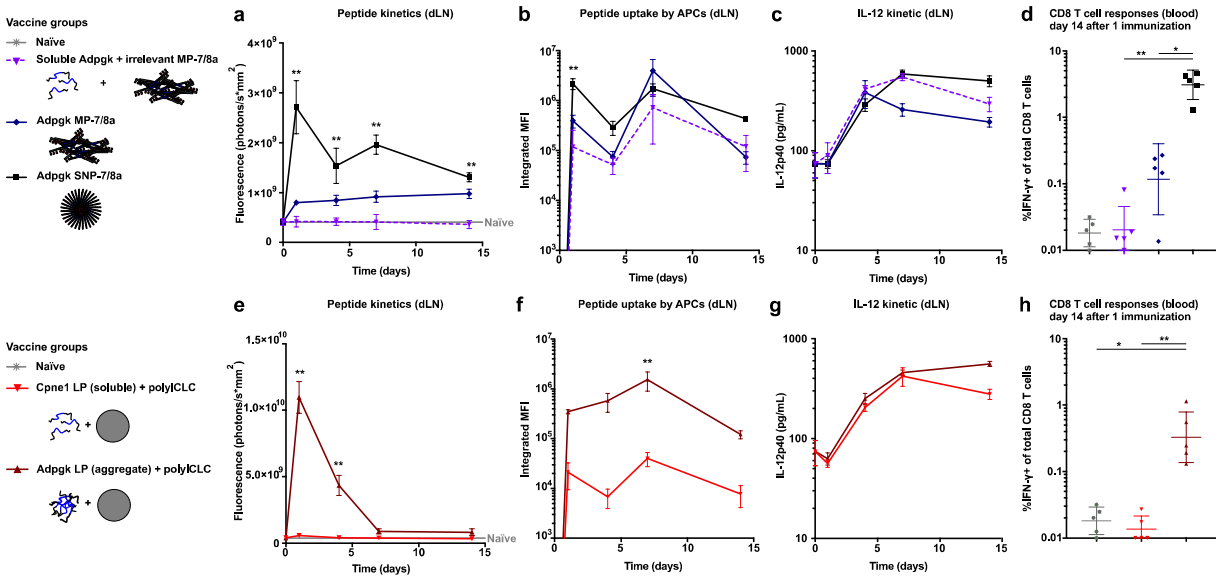

Figure 5: SNP-7/8a enhances antigen uptake by lymph node APCs.
(**a**–**d**) C57BL/6 mice (*n* = 5 per time point per group) were immunized with AlexaFluor647-labeled Adpgk Min either as the soluble peptide admixed with a particle TLR-7/8a (*i.e.*, MP-7/8a with an irrelevant antigen), as MP-7/8a, or as SNP-7/8a. Lymph nodes (*n* = 5 per group per time point) draining the site of immunization were collected at serial time points and assessed for (**a**) total tissue fluorescence (peptide quantity), (**b**) antigen uptake by APCs, and (**c**) IL-12p40 cytokine production. (**d**) CD8 T cell responses from blood were assessed by intracellular cytokine staining on day 14. (**e**–**h**) C57BL/6 mice (*n* = 5 per time point per group) were immunized with AlexaFluor647-labeled native LP neoantigens (Adpgk or Cpne1) admixed with polyICLC. Lymph nodes (*n* = 5 per group per time point) draining the site of immunization were collected and assessed as in **a**–**c** above. (**h**) CD8 T cell responses were assessed as in **d**. Data on log scale are reported as geometric mean with 95% c.i., except line graphs are reported as mean ± s.e.m. Statistical significance was determined using two-way ANOVA with Bonferroni correction (**a**–**c**, **e**–**f**) or Kruskal-Wallis with Dunn's correction (**d**,**f**); ns = not significant, **P* < 0.05, ***P* ≤ 0.01.

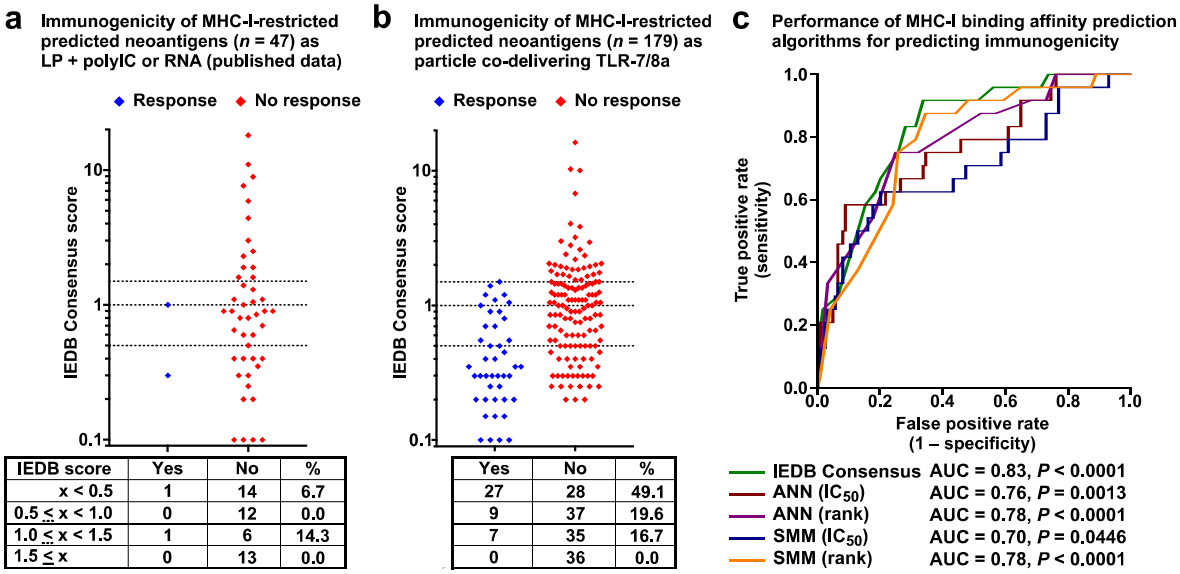

IEDB score	Yes	No	%
x < 0.5	1	14	6.7
0.5 ≤ x < 1.0	0	12	0.0
1.0 ≤ x < 1.5	1	6	14.3
1.5 ≤ x	0	13	0.0

Yes	No	%
27	28	49.1
9	37	19.6
7	35	16.7
0	36	0.0

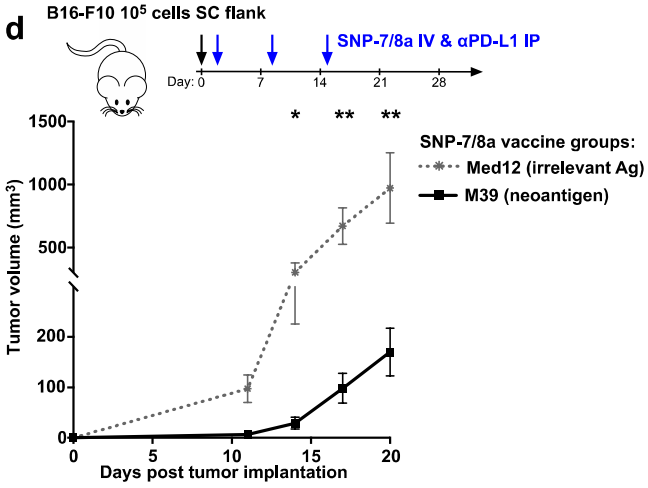

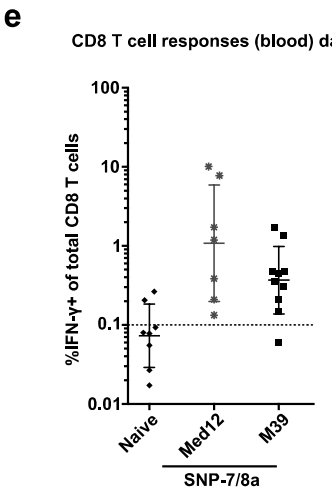

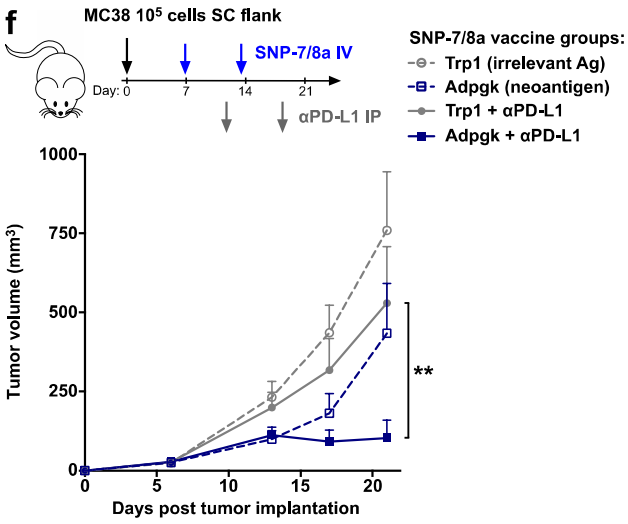

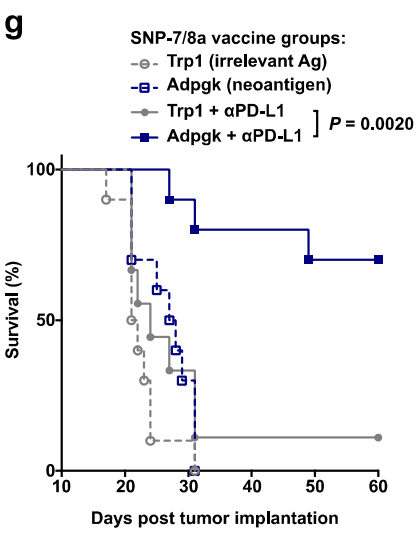

Figure 6: SNP-7/8a increases the breadth of neoantigen-specific CD8 T cell immunity. (**a**,**b**) Induction of neoantigen-specific CD8 T cell responses plotted against *in silico* predicted MHC-I binding affinity using the immune epitope database (IEDB) consensus algorithm. (**a**) CD8 T cell responses in mice vaccinated with predicted neoantigens (n = 47) derived from the B16-F10 tumor cell line as LP + polyIC or RNA, as described in ref. < Kreiter S, *et al. Nature* (2015)>. (**b**) CD8 T cell responses in mice for predicted neoantigens (n = 179) derived from the B16-F10, MC38, and SB-3123 tumor cell lines as peptide linked to oligo-7/8a. (**c**) Receiver operating characteristic curve showing performance of different algorithms for predicting MHC-I binding affinity for classifying neoantigens as immunogenic or non-immunogenic. (**d**,**e**) C57BL/6 mice (n = 10 per group) implanted subcutaneously with 1.0×10^5 B16-F10 tumor cells were vaccinated with SNP-7/8a delivering either Med12 (irrelevant antigen) or M39 (neoantigen) along with αPD-L1 on days 1, 8, and 15; (**d**) tumor growth was monitored at various time points, and (**e**) CD8 T cell responses were assessed from blood by intracellular cytokine staining on day 19. (**f**,**g**) C57BL/6 mice (n = 20 per group) implanted subcutaneously with 1.0×10^5 MC38 tumor cells were vaccinated intravenously with SNP-7/8a carrying the MC38 neoantigen Adpgk or an irrelevant antigen (Trp1) on days 7 and 13. Half the mice in each group additionally received αPD-L1 on days 12 and 19. (**f**) Tumor growth and (**g**) Kaplan-Meier survival curves (right) are shown. ANN = artificial neural network; SMM = stabilized matrix method. Data on log scale are reported as geometric mean with 95% c.i.; data on linear scale are reported at mean ± s.e.m. Statistical significance was determined using two-way ANOVA with Bonferroni correction (**d**,**f**) or Log-rank test with Bonferroni correction (**g**); ns = not significant, $*P < 0.05$, $**P \leq 0.01$.

ACKNOWLEDGEMENTS

The authors wish to acknowledge: M. Dillon, G. Salbador, L. Gilliam, C. Chiedi, and D. Scorpio of the Translational Research Program (VRC) as well as B. Klaunberg and V. Diaz at the Mouse Imaging Facility (MIF, NIH) for their valuable support with the animal studies; T. Abrams (VRC) for administrative support; Cytometry Platform and the Animal facilities of the Institut Curie; NSERM; Agence Nationale de la Recherche (ANR-11-LABX-0043 and ANR-10-IDEX-0001-02 PSL); Institut Curie (CIC IGR-Curie 1428); La Ligue Nationale Contre le Cancer program; SiRIC grant INCa-DGOS-12554; the Czech Science Foundation project 16-14957Y; and the Ministry of Education, Youth and Sports of the Czech Republic within the National Sustainability Program II (project BIOCEV-FAR LQ1604). This work was supported by the Intramural Research Program of the U.S. National Institutes of Health.

AUTHOR CONTRIBUTIONS

GL, CS, JB, OL, EP, AI, and RS contributed to planning experiments, interpreting the data and/or writing the manuscript. GL, YZ, VC, RL, and AI planned and carried out the synthesis, purification, and characterization of materials described in the manuscript. GL, CS, FB, AR-V, NZ, NB, KT, HY, JD, PR, BF, JC, JF, and AI planned and conducted many of the biological studies. BD conducted bioinformatics analyses. MS conducted brightfield imaging. MM conducted machine learning analysis. LS, CD, OL, EP, AI, and RS are lead investigators who advised the studies.

COMPETING FINANCIAL INTERESTS

GL, YZ, VC, RL, LS, AI, and RS are listed as inventors on patents describing polymer-based vaccines. GL, YZ, VC, BD, JB, and AI are employees/consultants of Avidea Technologies, Inc.

(Baltimore, MD), which is commercializing polymer-based drug delivery technologies for immunotherapeutic applications.

ONLINE METHODS

Animal protocols.

Animal experiments were conducted at the Vaccine Research Center (VRC) at the National Institutes of Health (Bethesda, MD) and the Institut Curie (Paris, France) and complied with the guidelines set by the Association for the Assessment and Accreditation of Laboratory Animal Care International (AAALAC) and the Institutional Animal Care and Use Committee (ACUC). All experimental animal protocols underwent review and were approved by the ACUC prior to the start of experiments.

Animals.

Female C57BL/6 (B6) mice were obtained from The Jackson Laboratory (Bar Harbor, ME) and maintained at the VRC Animal Care Facility (Bethesda, MD) under specific-pathogen-free conditions. B6 mice were 8–12 weeks of age at the start of experiments. Animals were randomly assigned to either control or experimental groups.

Peptide antigens.

Native peptide antigens and modified peptide antigens were custom synthesized by Genscript (Piscataway, NJ) using standard solid phase peptide synthesis and purified (>90%) by HPLC.

TLR-7/8 agonists and hydrophobic blocks (*e.g.*, oligo-7/8a).

Imidazoquinoline-based TLR-7/8 agonists were produced by Avidea Technologies, Inc. (Baltimore, MD) as previously described[1]. Detailed chemical schematics and descriptions of the methods used to synthesize and characterize the TLR-7/8a and hydrophobic blocks is provided in the Supplementary Materials and Methods.

Conjugate vaccine synthesis.

Conjugate vaccines were produced by linking peptide antigens to hydrophobic blocks (*e.g.*, oligo-7/8a) using a copper-free strain-promoted azide-alkyne cycloaddition click chemistry reaction. A detailed description of the methods used to synthesize and characterize the conjugate vaccines is provided in the Supplementary Materials and Methods.

Immunizations & treatment with checkpoint inhibitors.

Vaccines were prepared in sterile, endotoxin-free (<0.05 EU/mL) PBS (Gibco) and administered either subcutaneously in a volume of 50 μL in each hind footpad or intravenously via the tail vein in a volume of 200 μL. Adjuvants were either prepared in-house as previously described[1] and summarized in the Supplementary Materials and Methods or were acquired from commercial sources: polyIC (InvivoGen, San Diego, CA), anti-CD40 agonist (clone FGK4.5; BioXCell, West Lebanon, NH), and CpG 1826 (InvivoGen). PolyICLC (Hiltonol) was a kind gift of A. M. Salazar (Oncovir). Animals treated with checkpoint inhibitors (CPIs), αPD-1 (clone RMP1-14; BioXCell) and αPD-L1 (clone B7-H1; BioXCell) received 200 μg administered by the IP route in 100 μL PBS.

Tumor cell lines.

B16-F10 was acquired from ATCC (CRL-6475), MC38 was a kind gift from Lélia Delamarre (Genentech), TC-1 was a kind gift from T.C. Wu (Johns Hopkins University), and B16.OVA was a kind gift from H. Levitsky (Juno Therapeutics). Working cell banks (passage 4) were generated immediately upon receipt and used for tumor experiments. Cells were determined to be mycoplasma free upon establishment of each working cell bank.

Tumor implantations.

B16-F10, TC-1, and B16.OVA were cultured in RPMI-1640 media (GE Life Sciences), and

MC38 was cultured in DMEM media (Gibco), each supplemented with 10% v/v heat-inactivated FCS (Atlanta Biologicals), 100 U/mL penicillin, 100 μg/mL streptomycin (Gibco), 1× non-essential amino acids (GE Life Sciences), and 1 mM sodium pyruvate (GE Life Sciences). B16.OVA media was supplemented with 0.5 mg/mL G418. For each tumor cell implantation, a frozen aliquot was thawed, passaged once, and harvested using trypsin EDTA (Gibco), quenched with HI-FCS, washed in PBS, and implanted subcutaneously in sterile PBS. Tumors were measured using digital calipers twice per week, and tumor volume was estimated using the formula [tumor volume = short × short × long / 2]. Animals were euthanized when tumors reached size criteria (1000 mm^3 or 2000 mm^3).

CD8 depletion.

Mice were depleted for CD8 T cells by intraperitoneal injection of 250 μg of anti-CD8 (clone 2.43, BioXCell) in 100 μL PBS 1 d prior to tumor implantation, and 1 d and 7 d after tumor implantation. CD8 T cell depletion in the blood was confirmed using flow cytometry methods as described below.

Measurement of T cell responses by intracellular cytokine staining.

Measurement of antigen-specific CD8 and CD4 T cell responses by intracellular cytokine staining was performed as previously described[2]. Briefly, 200 μL heparin-treated whole blood was lysed with ACK lysis buffer (Quality Biologicals), filtered, and cultured in complete RPMI in 96-well plates with 2 μg/mL anti-CD28 (37.51, BD) in combination with 2 μg/mL of the native (unmodified) peptide antigen (Genscript). Brefeldin A (BFA, BD) was added to a final concentration of 10 μg/mL 2 h after purified peptides were added, and cells were incubated for an additional 4 h. After washing with PBS, cells were stained with UV Blue Live-Dead Dye (Life Technologies), washed, and blocked with anti-CD16/CD32 (clone 2.4G2, BD) for 10

minutes at room temperature. After blocking, cells were surface stained for 30 minutes at room temperature with BUV805-anti-CD8 (clone 53-6.7, BD) and BUV395-anti-CD4 (RM4-4, BD). Cells were then fixed and permeabilized using Fix / Perm solution (BD) and incubated at 4ºC for 30 minutes. Cells were washed and then suspended in Perm / Wash buffer containing AlexaFluor700-anti-CD3 (17A2, BioLegend), APC-anti-IFN-γ (XMG1.2, BD), PE-anti-IL-2 (JES6-5H4, BD) and BV650-anti-TNFα (MP6-XT22, BD) for 30 minutes at 4ºC for 30 minutes. Cells were washed and suspended in 0.5% paraformaldehyde (Electron Microscopy Sciences) in PBS and then evaluated by flow cytometry.

Multimer (tetramer/dextramer) staining of CD8 T cells from whole blood.

Tetramer+ or dextramer+ CD8 T cell responses were characterized from whole blood as previously described[3]. Briefly, 200 µL heparin-treated whole blood was lysed with ACK lysis buffer, filtered, and plated in 96-well plates in PBS. Cells were stained with the viability dye Live/Dead Fixable Orange (OrViD, Life Technologies) for 10 minutes at room temperature. After washing, cells were stained for 15 minutes at 4°C with PE-H2-K^b OVA (SIINFEKL) tetramer (Beckman Coulter, Brea, California) or with PE-H2-D^b Reps1 (AQLANDVVL) or Irgq (AALLNSAVL) dextramers (Immudex, Copenhagen, Denmark). Cells were then blocked with anti-CD16/CD32 (clone 2.4G2, BD) for 10 minutes, followed by the addition of APC-Cy7-anti-CD8 (53-6.7, Biolegend), PE-Cy7-anti-CD62L (MEL-14, Abcam, Cambridge, England), eFluor-660-anti-CD127 (A7R34, eBioscience) and FITC-anti-KLRG1 (2F1, Southern Biotech, Birmingham, Alabama). After incubating for 20 minutes at room temperature, cells were washed and then incubated with Fix / Perm solution (BD) for 20 minutes at 4°C. After washing, cells were suspended in Perm / Wash buffer containing PerCP-Cy5.5-anti-CD3 (145-2C11, BD) and

incubated at 4°C for 30 minutes. Cells were washed and suspended in Perm / Wash buffer and then evaluated by flow cytometry.

Flow cytometry.

Samples were acquired on a modified BD LSR Fortessa X-50 flow cytometer. Results were analyzed using FlowJo v9.9.6 (TreeStar).

Characterization of innate immune cells and cytokines from lymph nodes.

The uptake of AlexaFluor647-labeled vaccines by antigen presenting cells (APCs) in the vaccine-draining popliteal lymph nodes (dLN) were evaluated as previously described[1]. Briefly, dLN of vaccinated mice were harvested at specified time points and mechanically disrupted in BioMasher tubes (Nippi Inc, Japan) containing PBS. Resulting cell suspensions were filtered through a 40 μm nylon mesh filter plate (EMD Millipore). Half of each dLN cell suspension was incubated at 37°C in complete RPMI for 12 hours. Supernatants were harvested and IL-12p40 concentration was determined by quantitative ELISA (Peprotech). The other half of each dLN cell suspension was transferred to V-bottom 96-well plates (Sigma Aldrich) for staining. Cells were stained for 10 minutes at room temperature with Live/Dead Fixable Aqua (Life Technologies), washed, and blocked with anti-CD16/CD32 (clone 2.4G2, BD) for 10 minutes at room temperature. After blocking, cells were surface stained with BV510-anti-CD3 (145-2C11, BD), BV421-anti-CD19 (1D3, BD), BV605-anti-Ly-6G (1A8, BD), BV786-anti-CD8 (53-6.7, BD), BV510-anti-NK-1.1 (PK136, BD), Cy7-PE-anti-B220 (RA3-6B2, BD), AlexaFluor488-anti-I^A/I^E (M5/114.15.2, Biolegend), PE-anti-CD11c (HL3, BD), AlexaFluor700-anti-CD11b (M1/70, BioLegend), Cy5-PE-anti-F4/80 (BM8, eBioscience), and CF594-PE-anti-CD80 (16-10A1, BD). Cells were washed, fixed in 0.5% paraformaldehyde in PBS, and analyzed by flow cytometry. The integrated median fluorescence intensity (iMFI) was calculated by multiplying

the total number of cells positive for the vaccine (AlexaFluor647+ cells) and the Median Fluorescence Intensity of the AlexaFluor647+ cells.

Quantification of vaccine in draining lymph nodes by fluorescence measurements.

Single cell suspensions of lymph nodes were added to black-walled 96-well plates and quantified for AlexaFluor647-labeled vaccines by performing epifluorescence imaging (excitation = 650 nm; emission = 700 nm; 0.50 second exposure) using a Bruker In Vivo Xtreme (Bruker, Billerica, MA); fluorescence was determined by placing identically-sized regions of interest over each well.

Evaluation of OT-I expansion *in vivo*.

The duration of antigen presentation following vaccination was assessed by measuring the expansion of OT-I cells adoptively transferred into vaccinated mice. OT-I cells were prepared by isolating total CD8+ T cells from spleen and lymph nodes of OT-I transgenic CD45.1 mice using Miltenyi beads (Bergisch Gladbach, Germany). The OT-I CD8 T cells were then labeled with 5 μM CFSE (carboxyfluorescein succinimidyl ester, Life Technologies) in PBS containing 0.1% BSA (Bovine Serum Albumin, Sigma-Aldrich) for 8 min at 37°C. CFSE-labeled OT-I cells (1×10^6) were injected intravenously (i.v.) in 100 μL PBS 0.1% BSA at different time points (day 0, 3, or 7) after C57BL/6 CD45.2 mice were injected subcutaneously with the indicated vaccines. Analysis of the *in vivo* expansion was performed 6 days after adoptive transfer by enumerating the number of CFSE-diluted CD8+ CD45.1+ OT-I cells from draining lymph nodes cells of vaccinated mice.

Prediction of MHC-I binding affinity and immunogenicity screens.

Mutations resulting from a single-nucleotide polymorphism that were also transcribed in a mouse tumor were selected from MC38 (Ref.[4]), B16-F10 (Nina Bhardwaj, personal communication),

and SB-3123 cell line (Nicholas Restifo, personal communication) without confirmation of MHC-I binding. Binding affinity for each peptide was predicted using Immune Epitope Database (IEDB) Consensus algorithm v2013-02-22 (ref.[5]), the ANN method[6], and the SMM method[7]. Predictions were made for both H2-K^b and H2-D^b MHC-I alleles, and the higher predicted binding affinity of the two alleles was selected for subsequent regression analysis. Each epitope (n = 179) selected for analysis was prepared as a peptide antigen linked to oligo-7/8a. Mice (n = 5 per group) were vaccinated subcutaneously in two sites with a pool of four antigens (1 nmol per antigen per site) on days 0 and 14. CD8 T cell responses were assessed 7 days after final vaccination for each antigen individually by ICS as described above. If any antigen in a pool was positive, each of the four antigens were then tested separately to confirm immunogenicity.

Hydropathy and charge frequency distribution of human neoantigens.

All available human protein sequences were downloaded from Ensembl 2017 (ref.[8]). Canonical transcripts were identified as the longest sequence for each unique Ensembl protein-coding gene identifier. All possible wild type 25-mer peptides (n = 11.3M) were extracted from canonical protein sequences using a bespoke Python script. All possible single nucleotide mutations resulting in a missense substitution were identified using the database for non-synonymous functional prediction (dbNSFP; ref. [9]). All possible 25-mer peptides incorporating a single missense mutation were then extracted (n = 72.6M). The net charge (K, R = +1; E, D = –1; all other amino acids = 0) and grand average of hydropathy (GRAVY)[10] were calculated for each wild type and mutant peptide.

Machine learning model.

A random forest machine learning model[11] was used to predict whether a given conjugate vaccine would form nanoparticles (as assessed by turbidity < 0.05) or larger particles (turbidity >

0.05) based on measured and derived properties of the underlying composition (net charge, hydropathy, lengths of the constituent structural elements). 10-fold cross-validated models were derived to avoid overfitting the data. In each of these cross-validations, the random forest hyperparameters (the number of trees and the number of variables considered at each split) were tuned via Gaussian process optimization (*scikit-optimize: Sequential model-based optimization*, GitHub, 2018). To avoid overfitting the hyperparameters, their tuning was performed with 5-fold cross-validation, in 100 iterations (including 10 initial steps where the hyperparameters were set randomly), controlled by the log-loss. The resulting 10-fold cross-validated out-of-sample ROC curves and average ROC were reported.

Statistics and graphs.

Sample sizes for biological studies were chosen based on calculations using JMP statistical analysis software (Cary, NC); standard deviations and pre-specified differences in groups ("differences to detect") were based on historical data, and type I and type II error rates were set at 0.05 and 0.2, respectively. Unless stated otherwise, data on linear axes are reported as mean ± s.e.m. Data on log scale are reported as geometric mean with 95% c.i. Statistical analyses were carried out using Prism software (GraphPad). Unless stated otherwise within the figure legends, Kruskal-Wallis one-way ANOVA with Dunn's post-test correction for multiple comparisons was used to calculate *P*-values for comparisons between > 2 groups; two-way ANOVA with Bonferroni correction was used to calculate *P*-values for comparisons between groups over multiple time points; and log rank test was used to compare survival differences for Kaplan-Meier plots.

ONLINE METHODS REFERENCES

1 Lynn, G. M. *et al.* In vivo characterization of the physicochemical properties of polymer-linked TLR agonists that enhance vaccine immunogenicity. *Nat Biotechnol* **33**, 1201-1210, doi:10.1038/nbt.3371 (2015).

2 Darrah, P. A. *et al.* Multifunctional TH1 cells define a correlate of vaccine-mediated protection against Leishmania major. *Nature medicine* **13**, 843-850, doi:10.1038/nm1592 (2007).

3 Quinn, K. M. *et al.* Comparative analysis of the magnitude, quality, phenotype, and protective capacity of simian immunodeficiency virus gag-specific CD8+ T cells following human-, simian-, and chimpanzee-derived recombinant adenoviral vector immunization. *J Immunol* **190**, 2720-2735, doi:10.4049/jimmunol.1202861 (2013).

4 Yadav, M. *et al.* Predicting immunogenic tumour mutations by combining mass spectrometry and exome sequencing. *Nature* **515**, 572-576, doi:10.1038/nature14001 (2014).

5 Kim, Y. *et al.* Immune epitope database analysis resource. *Nucleic Acids Res* **40**, W525-530, doi:10.1093/nar/gks438 (2012).

6 Nielsen, M. *et al.* Reliable prediction of T-cell epitopes using neural networks with novel sequence representations. *Protein Sci* **12**, 1007-1017, doi:10.1110/ps.0239403 (2003).

7 Peters, B. & Sette, A. Generating quantitative models describing the sequence specificity of biological processes with the stabilized matrix method. *BMC Bioinformatics* **6**, 132, doi:10.1186/1471-2105-6-132 (2005).

8 Aken, B. L. *et al.* Ensembl 2017. *Nucleic Acids Res* **45**, D635-D642, doi:10.1093/nar/gkw1104 (2017).

9 Liu, X., Wu, C., Li, C. & Boerwinkle, E. dbNSFP v3.0: A One-Stop Database of Functional Predictions and Annotations for Human Nonsynonymous and Splice-Site SNVs. *Hum Mutat* **37**, 235-241, doi:10.1002/humu.22932 (2016).

10 Kyte, J. & Doolittle, R. F. A simple method for displaying the hydropathic character of a protein. *J Mol Biol* **157**, 105-132 (1982).

11 Liaw, A. & Wiener, M. Classification and Regression by randomForest. *R News* **2**, 18-22, doi:citeulike-article-id:1121494 (2002).

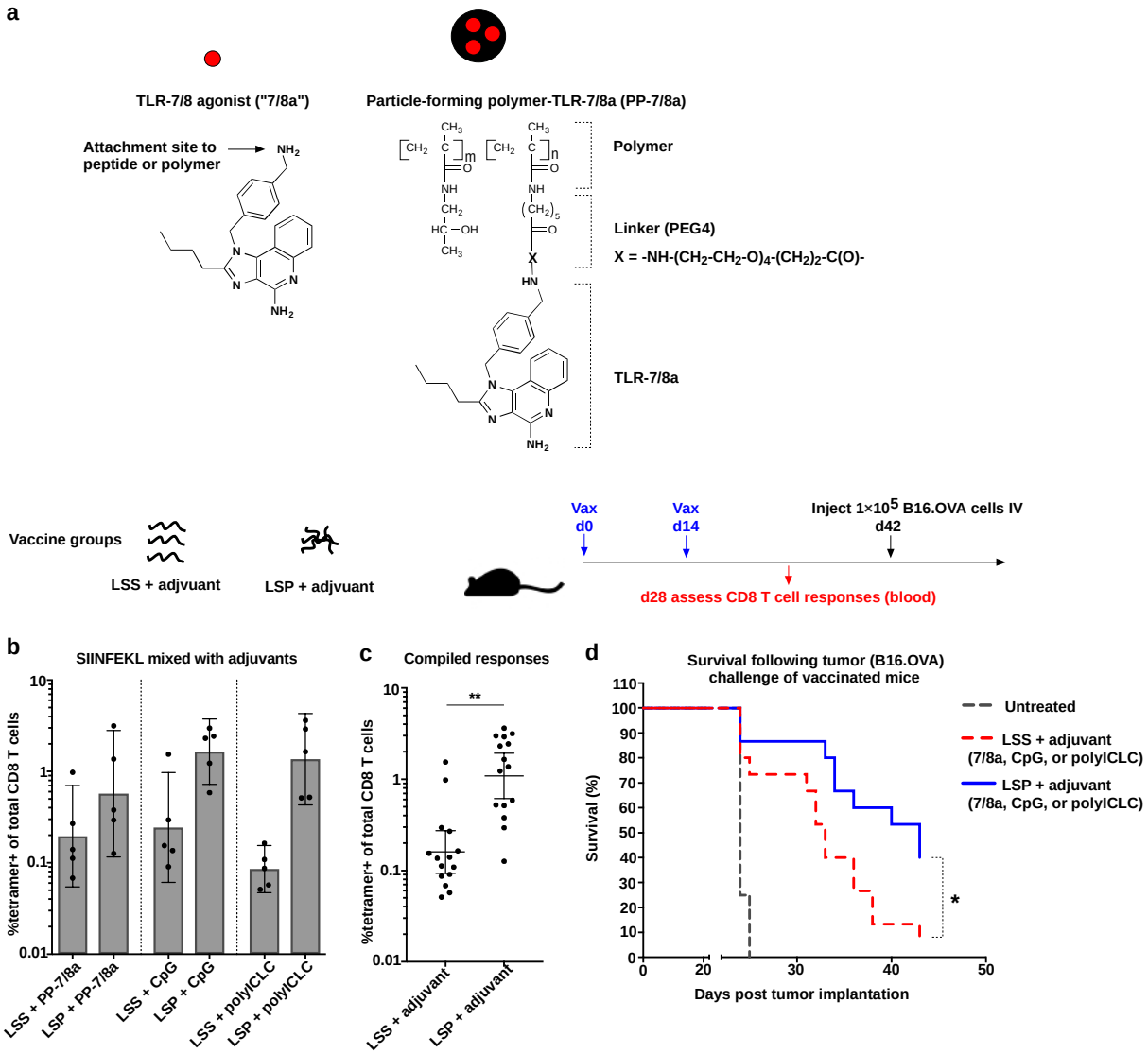

Extended Data Fig. 1: Efficiency of CD8 T cell induction depends on LP physical form. (**a**) Chemical schematics of the imidazoquinoline-based Toll-like receptor-7 & -8 agonist (TLR-7/8a) that was linked to the SIINFEKL LPs (LSS-7/8a and LSP-7/8a) and of the particle-forming polymer-TLR-7/8a (PP-7/8a). (**b**–**d**) C57BL/6 mice (n = 5 per group) were immunized with LSS or LSP admixed with either PP-7/8a, CpG, or polyICLC at days 0 and 14. (**b**) Tetramer+ CD8 T cell responses were assessed by flow cytometry on day 28 for each adjuvant, and (**c**) grouped for comparison. (**d**) C57BL/6 mice vaccinated with either LSS or LSP mixed with adjuvant (n = 15 per group) were challenged with B16.OVA on day 42 and assessed for survival. Data on log scale are reported as geometric mean with 95% c.i.; data on linear scale are reported as mean ± s.e.m. Comparison of multiple groups for statistical significance was determined using Kruskal-Wallis with Dunn's correction; statistical significance of survival was determined using Log-rank test; ns = not significant, *$P < 0.05$, **$P \leq 0.01$.

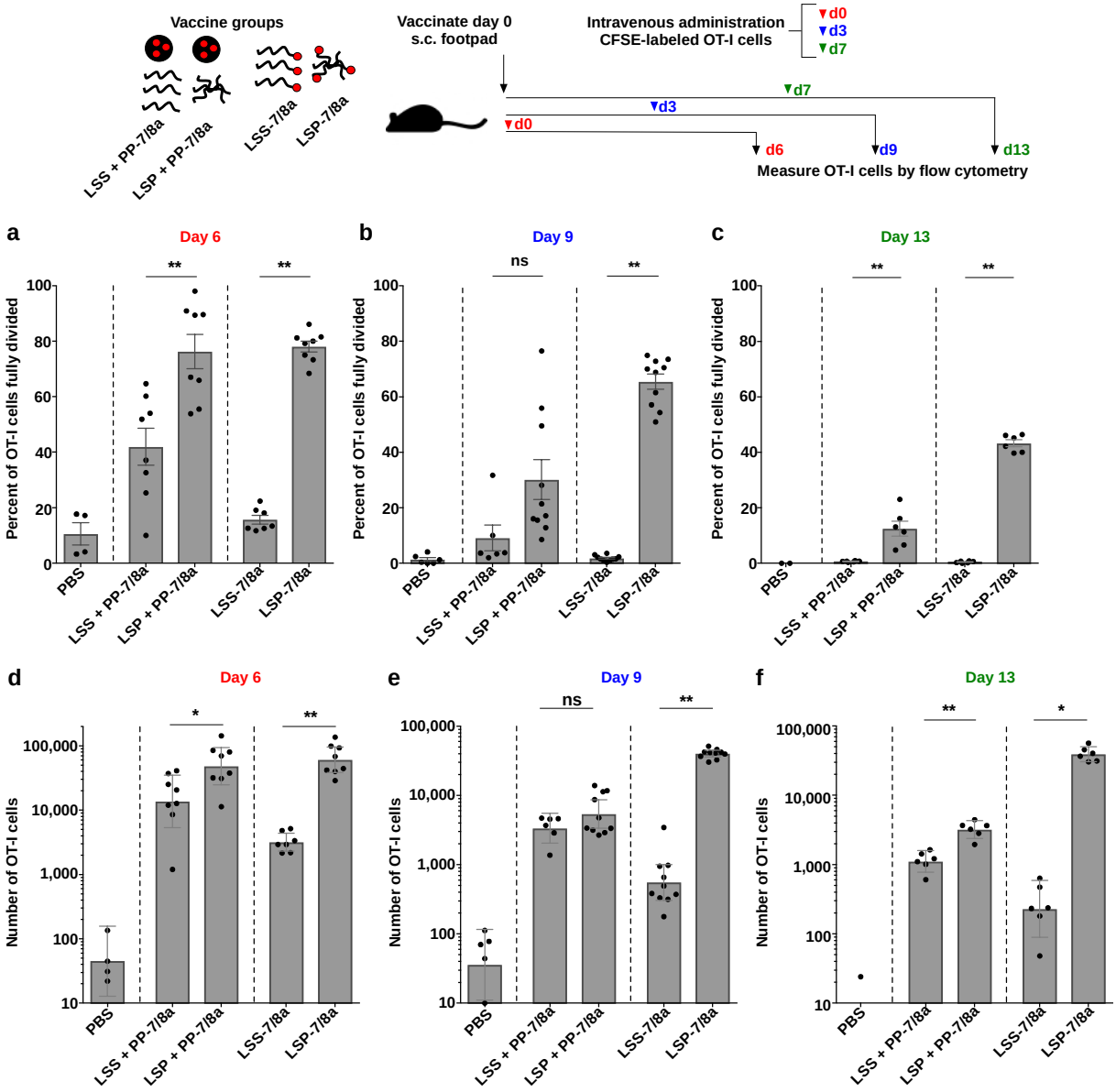

Extended Data Fig. 2: Particulate LPs prolong antigen presentation *in vivo* leading to higher frequencies of antigen-specific CD8 T cells.

(**a**–**f**) Three separate cohorts of C57BL/6 mice (n = 5–8 per group per time point) were immunized with LSS or LSP, either admixed with PP-7/8a or covalently linked to TLR-7/8a (LSS-7/8a and LSP-7/8a). CFSE-labeled OT-I cells were then administered intravenously to each cohort on day 0, 3, or 7, as shown diagrammatically. Six days after receiving the OT-I cells, the percent of OT-I cells that fully divided (**a**–**c**) and total number of OT-I cells (**d**–**f**) were determined by flow cytometry. Data on linear scale are reported as mean ± s.e.m; data on log scale are reported as geometric mean with 95% c.i. Comparison of multiple groups for statistical significance was determined using Kruskal-Wallis with Dunn's correction; ns = not significant, *$P < 0.05$, **$P \leq 0.01$.

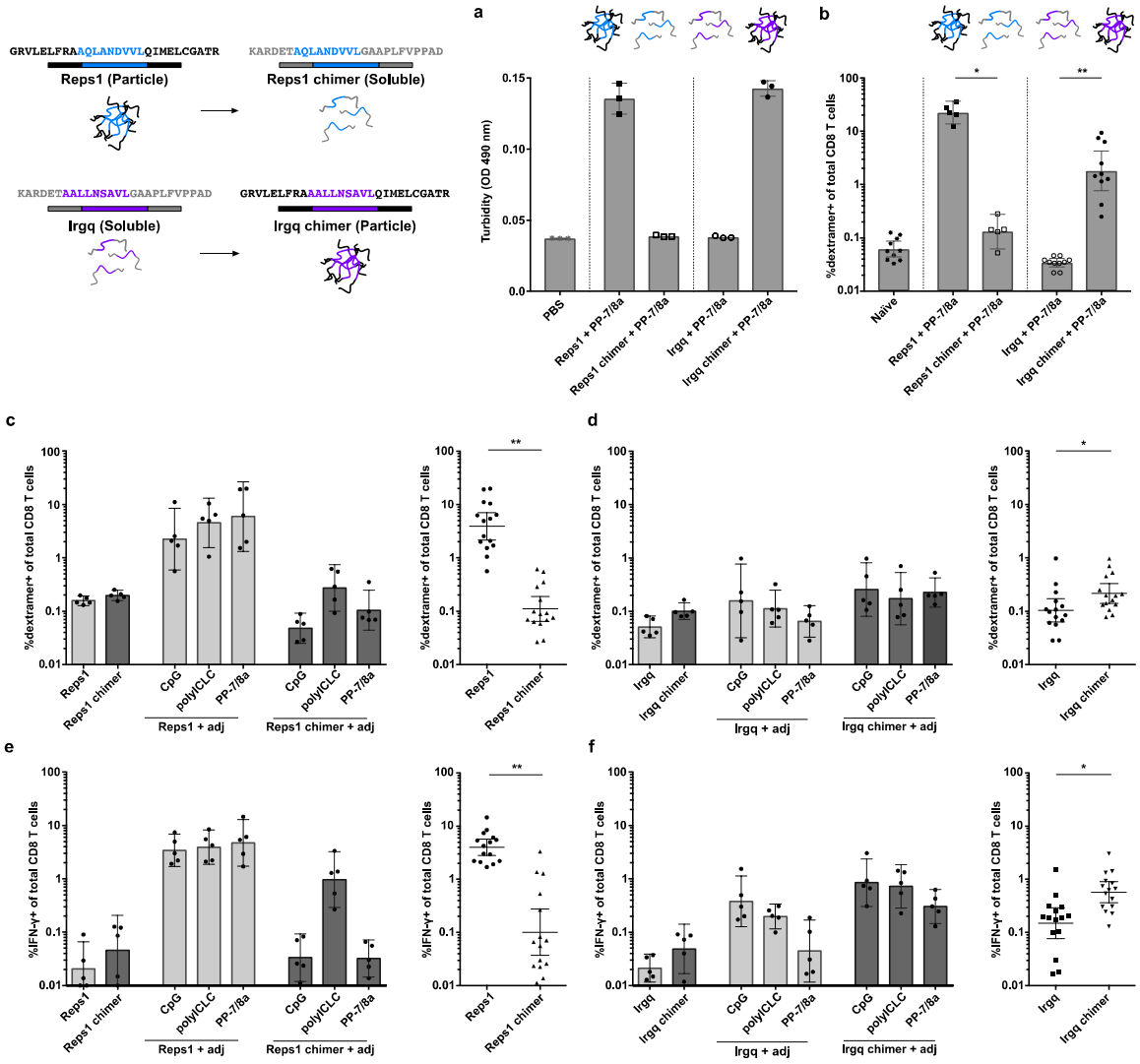

Extended Data Fig. 3: Particulate but not soluble neoantigen LPs induce CD8 T cell responses.

(**a**–**f**) The amino acid residues flanking the minimal epitopes of Reps1 (AQLANDVVL) and Irgq (AALLNSAVL) neoantigens were exchanged to generate Reps1 and Irgq chimers. (**a**) Turbidity, as measured by the absorbance of light at 490 nm, was used to assess whether different LPs aggregate (OD > 0.05) or are soluble (OD ≤ 0.05) in aqueous solution. (**b**–**f**) Native and chimeric forms of Reps1 and Irgq LP neoantigens were admixed with different adjuvants (*i.e.*, PP-7/8a, CpG, or polyICLC) and administered to C57BL/6 mice (n = 5–10 mice per group) at days 0 and 14 and CD8 T cell responses were assessed by either (**b**–**d**) dextramer staining (AQLANDVVL-H-2D^b or AALLNSAVL-H-2D^b) or (**e**,**f**) IFN-γ intracellular cytokine staining of blood on day 28. Data on linear scale are reported as mean ± s.e.m; data on log scale are reported as geometric mean with 95% c.i. Comparison of multiple groups for statistical significance was determined using Kruskal-Wallis with Dunn's correction; Mann-Whitney test was used to assess significance for comparison of compiled responses in figure panels **c**–**f**; ns = not significant, *P < 0.05, **$P \leq 0.01$.

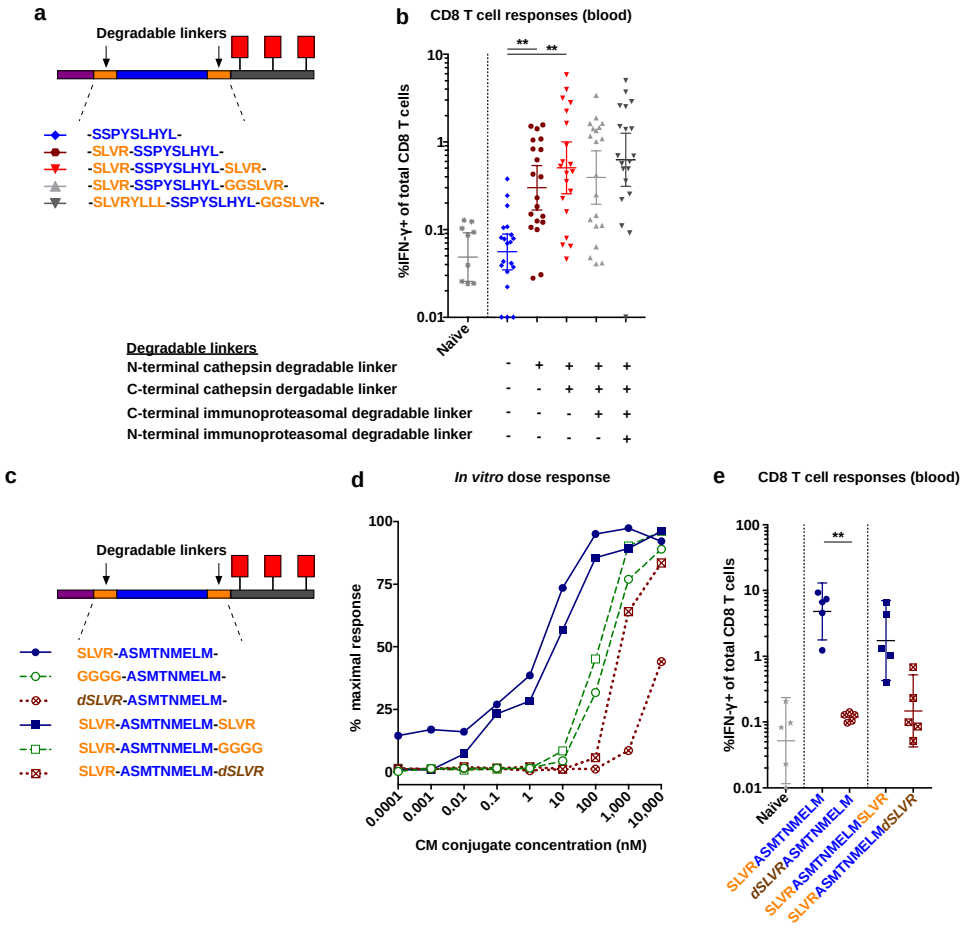

Extended Data Fig. 4: Effect of enzyme degradable linker composition on antigen presentation and CD8 T cell priming.

(**a**,**b**) An MHC-I (H-2D^b)-restricted epitope (SSPYSLYHL) from the MC38 tumor cell line-derived neoantigen, Cpne1, was linked at the N-terminus to a charge modifying group either directly or through enzyme (cathepsin, or cathepsin and proteasome) degradable peptide linkers, and at the C-terminus to an oligo-7/8a either directly or through enzyme (cathepsin, or cathepsin and proteasome) degradable linkers. (**b**) C57BL/6 mice (n = 20 per group) were immunized with the SSPYSLYHL CM conjugates of varying degradable linker composition on day 0 and CD8 T cell responses from blood were assessed by intracellular cytokine staining on day 7. Addition of cathepsin degradable linkers significantly increased the CD8 T cell response, which was not further increased with addition of linkers that are also recognized by the proteasome. (**c**–**e**) An MHC-I (H-2D^b)-restricted epitope (ASMTNMELM) from the MC38 tumor cell line neoantigen, Adpgk, was prepared as either a CM conjugate with a cathepsin degradable linker (SLVR) at the N-terminus or both the N- and C-termini; alternatively, the cathepsin degradable linker was replaced with a non-specific sequence (GGGG) or with D amino acids (dSLVR). (**d**) *In vitro* antigen presentation as assessed by titrating the indicated CM conjugates with ASMTNMELM-specific CD8 T cells and measuring the IFN-γ response by intracellular cytokine staining. (**e**) *In vivo* priming of CD8 T cells by the indicated CM conjugates. Note: use of the D-chirality amino acid (*i.e.* dSLVR) abrogates activity. Data on log scale are reported as geometric mean with 95% c.i. Comparison of multiple groups for statistical significance was determined using Kruskal-Wallis with Dunn's correction; ns = not significant, *$P < 0.05$, **$P \leq 0.01$.

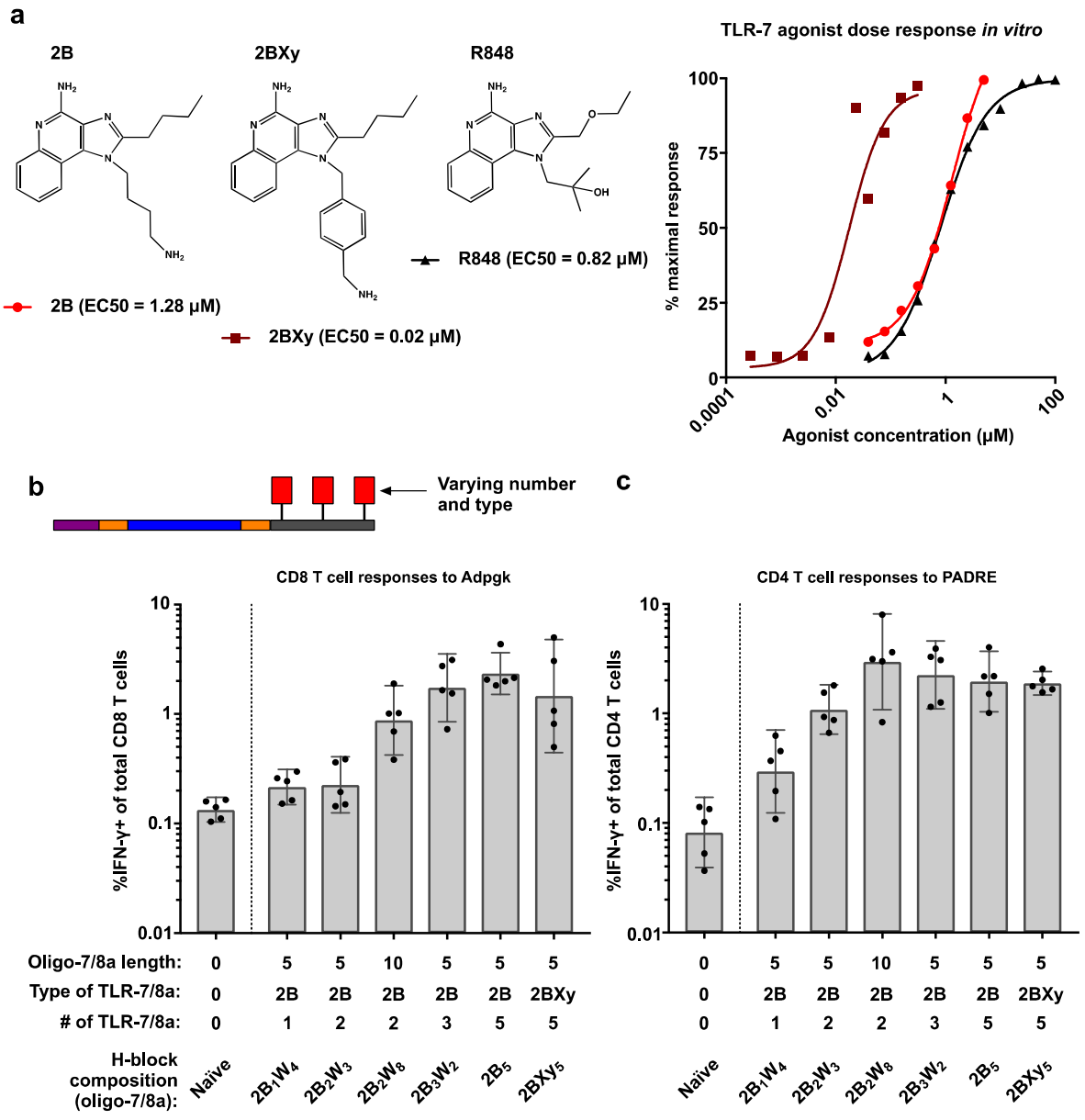

Extended Data Fig. 5: Impact of the number and type of TLR-7/8a on T cell responses. (**a**) Chemical structures and *in vitro* dose response curves for the conjugatable imidazoquinoline TLR-7/8 agonists "2B" (EC_{50} = 1.28 μM) and "2BXy"(EC_{50} = 0.02 μM). Potency was determined via a colorimetric reporter assay by incubating different concentrations of TLR-7/8a with HEK293 cells expressing human TLR-7 and a reporter enzyme, SEAP (InvivoGen cat #hkb-htlr7). R848 ("Resiquimod") is shown for comparison. (**b**–**c**) C57BL/6 mice (n = 5 per group) were immunized with either (**b**) the Adpgk minimal epitope (ASMTNMELM) or (**c**) a model CD4 T cell epitope (AKFVAAWTLKAAA, "PADRE") as charge-modified (CM) conjugates comprising different compositions of oligo-7/8a. Blood was collected on day 22 and assessed for IFN-γ-producing T cells by intracellular cytokine staining. Data on log scale are reported as geometric mean with 95% c.i.

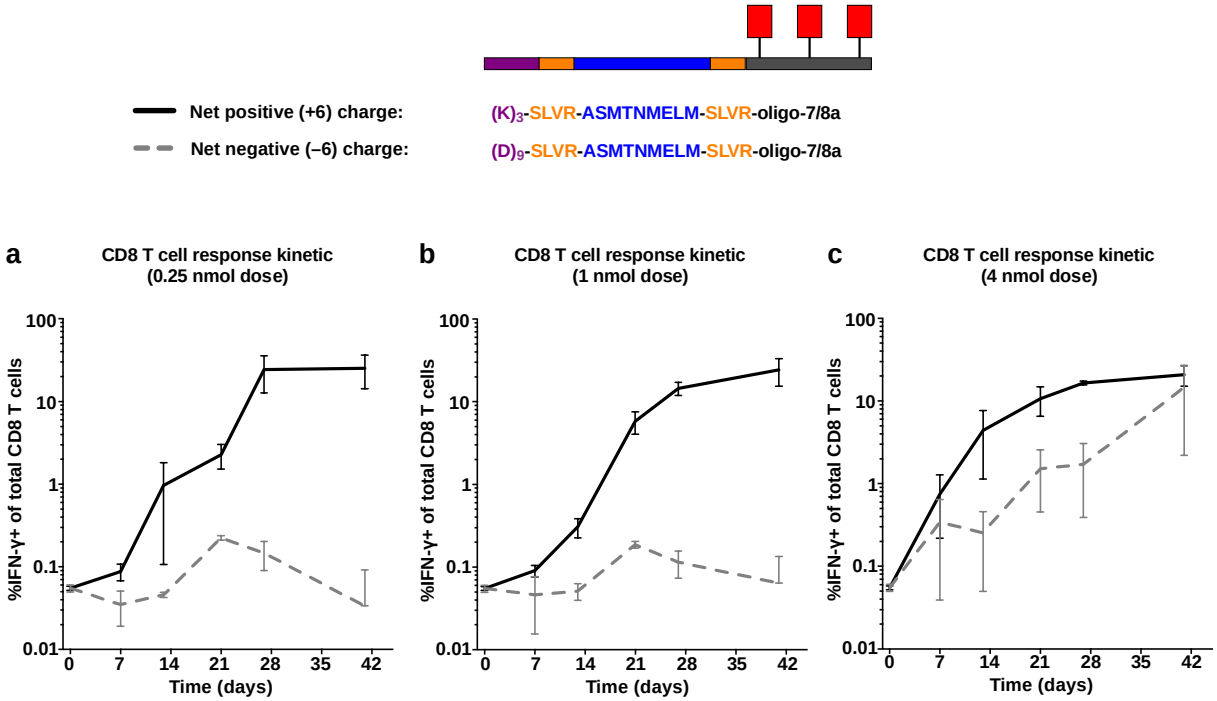

Extended Data Fig. 6: Impact of net charge on CD8 T cell responses.
(**a**–**c**) An MHC-I (H-2D^b)-restricted epitope (ASMTNMELM) from the MC38 tumor cell line derived neoantigen, Adpgk, was prepared as a charged-modified (CM) conjugate with either net positive (+6) or net negative (–6) charge. The positive and negatively charged CM conjugates were administered subcutaneously to mice (n = 3 per group per dose) at days 0, 14, and 28 at doses of either (**a**) 0.25 nmol, (**b**) 1 nmol, or (**c**) 4 nmol per vaccination, and CD8 T cell responses from blood were evaluated by intracellular cytokine staining at the time points shown. Data are reported as mean ± s.e.m.

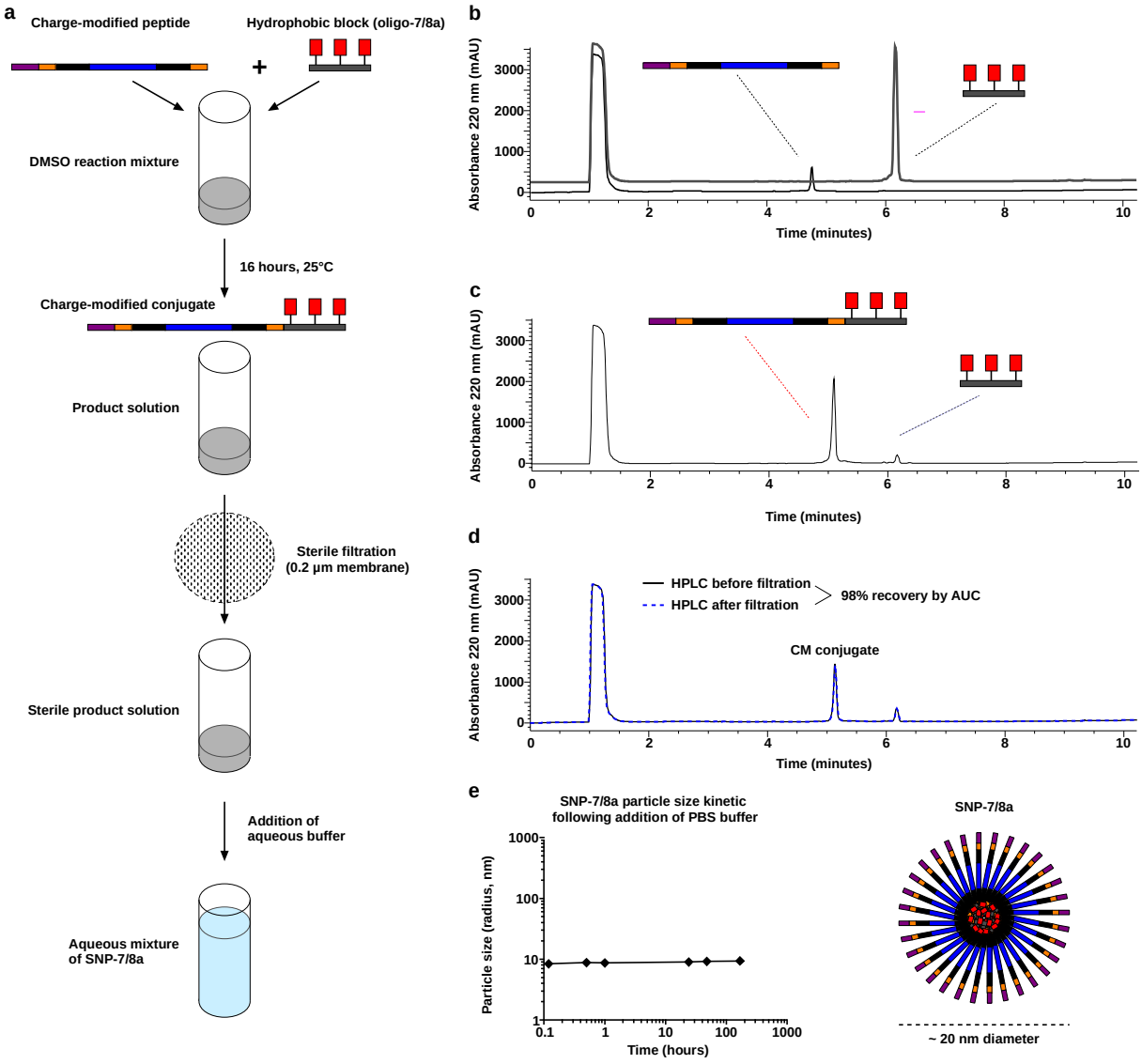

Extended Data Fig. 7: Manufacturing workflow for PCVs based on SNP-7/8a.
(**a**) Schematic of the manufacturing workflow for production of a PCV. Each CM peptide comprises a patient-specific neoantigen and is produced on-demand by solid-phase peptide synthesis. The hydrophobic block (oligo-7/8a) is the same for each patient and manufactured in bulk. Each patient-specific CM peptide is reacted with the oligo-7/8a in DMSO at room temperature for 16h to yield a CM conjugate product solution. The product solution is sterile filtered to produce a sterile product solution. Addition of aqueous buffer to the sterile product solution results in the CM conjugates self-assembling into nanoparticles. (**b**) Representative HPLC chromatograms of a CM peptide and oligo-7/8a. Representative HPLC chromatograms of a product solution (**c**) and sterile product solution (**d**). Overlaying the chromatogram prior to and after sterile filtration indicates that no significant change in composition has occurred. (**e**) SNP-7/8a particle size over time following addition of PBS pH 7.4 to a sterile product solution comprising a CM conjugate.

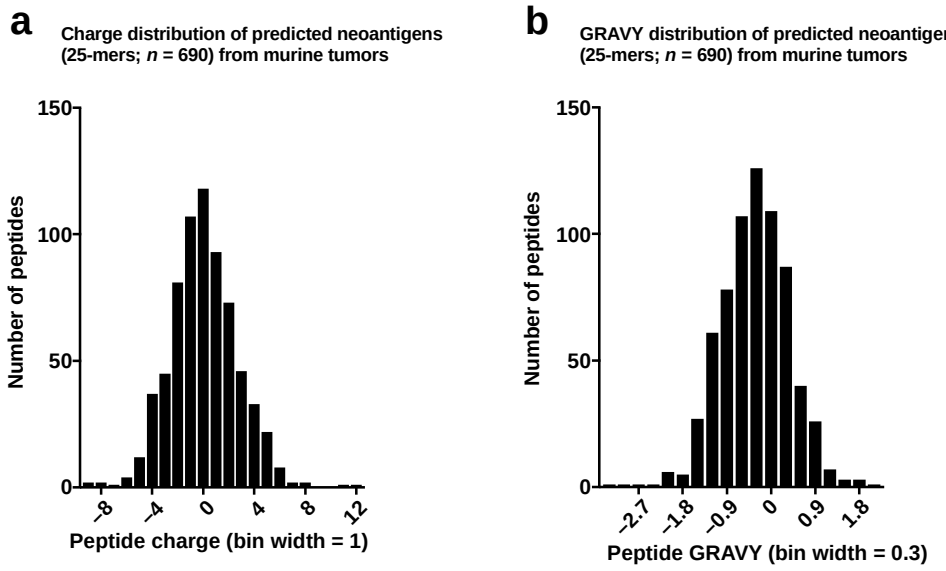

Extended Data Fig. 8: Charge and hydropathy distribution of predicted neoantigens derived from mouse tumor models.
(**a**) Charge and (**b**) grand average of hydropathy (GRAVY) distribution plots for *n* = 690 LP neoantigens derived from 3 mouse tumor models (B16-F10, MC38, and SB-3123).

a SNP-7/8a with 20 different CM conjugates

#	Neoantigen sequence	Charge	GRAVY
1	GIPVHLELASMTNMELMSSIVHQQVFPT	−2	0.43
2	GRVLELFRAAQLANDVVLQIMELCGATR	0	0.52
3	DFTGSNGDPSSPYSLHYLSPTGVNEY	−3	−0.82
4	KARDETAALLNSAVLGAAPLFVPPAD	−1	0.38
5	EAGQSLVISASIIVFNLLELEGDYR	−3	0.54
6	SKLLSFMAPIDHTTMSDDARTELFRS	−1	−0.31
7	RDIDPSSSVLFEYMEKPDFSLFSP	−3	−0.39
8	TAKSVMCTYSPPLDKLFCQLAKTCPVQ	2	0.13
9	VVDRNPQFLDPVLAYLMKGLCEKPLAS	0	0.20
10	RSSPDEVALVEGVQSLGFTYLRLKDNYM	−1	−0.28
11	IPSGTTILNCFHDVLSGKLSGGSPGVP	0	0.32
12	DSGSPFPAAVILRDALHMARGLKYLHQ	1	−0.03
13	NREKMKGELGMMLILQNVIQKTTTPGE	1	−0.57
14	EKFSMDHKTGTIAMQNTTQLRSRYELT	1	−1.01
15	RREGVELCPGNKYEMRRHGTTHSLVIHD	1	−1.09
16	MAAALTFRRLLTLPRAARGFGVQVS	4	0.56
17	LCSEPMFTFVYPTIFPLRETPMAGL	−1	0.56
18	AWHTNLSRKILRMSPLLAKFHQFLV	4	0.15
19	KGFELLYQPEVVHLYLSLLTESRNF	−1	0.03
20	SFVRQLNMYGFRNVVHIESGIIKQE	1	−0.14

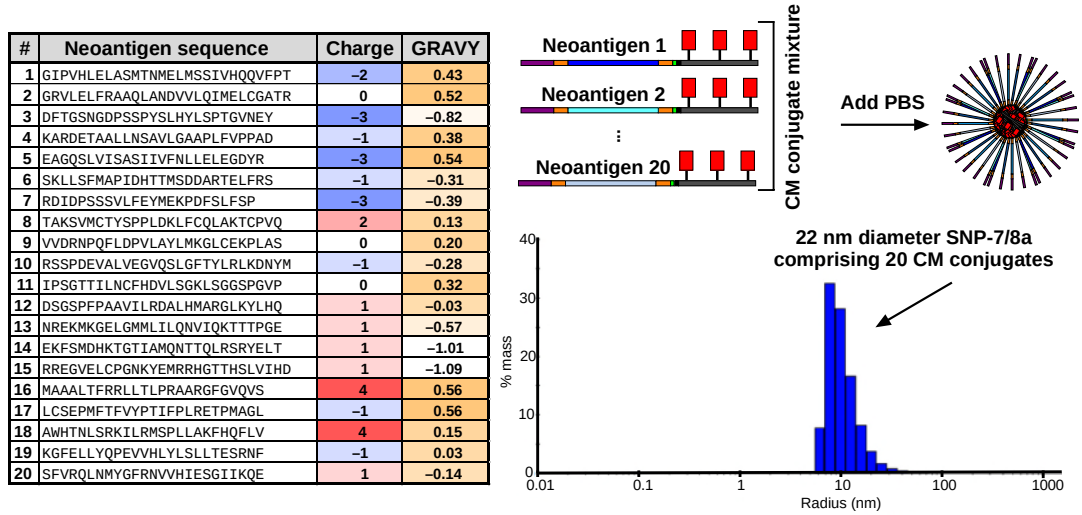

b Hydrodynamic properties of SNP-7/8a comprising different CM conjugate compositions

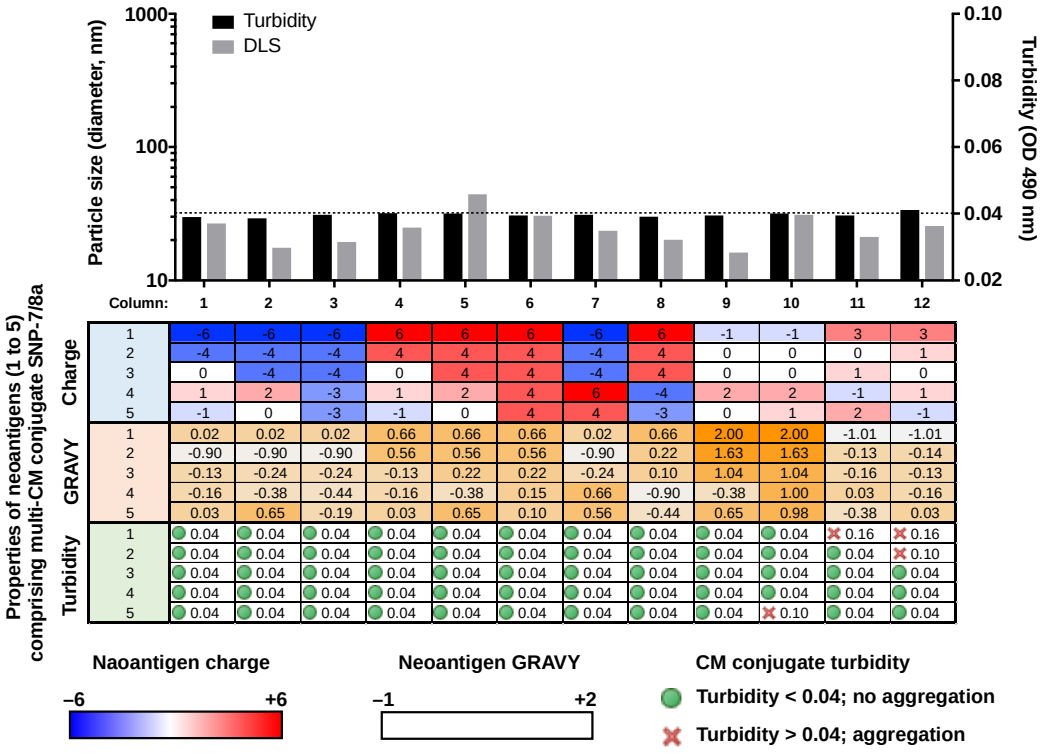

		1	2	3	4	5	6	7	8	9	10	11	12
Charge	1	-6	-6	-6	6	6	6	-6	6	-1	-1	3	3
	2	-4	-4	-4	4	4	4	-4	4	0	0	0	1
	3	0	-4	-4	0	4	4	-4	4	0	0	1	0
	4	1	2	-3	1	2	4	6	-4	2	2	-1	1
	5	-1	0	-3	-1	0	4	4	-3	0	1	2	-1
GRAVY	1	0.02	0.02	0.02	0.66	0.66	0.66	0.02	0.66	2.00	2.00	-1.01	-1.01
	2	-0.90	-0.90	-0.90	0.56	0.56	0.56	-0.90	0.22	1.63	1.63	-0.13	-0.14
	3	-0.13	-0.24	-0.24	-0.13	0.22	0.22	-0.24	0.10	1.04	1.04	-0.16	-0.13
	4	-0.16	-0.38	-0.44	-0.16	-0.38	0.15	0.66	-0.90	-0.38	1.00	0.03	-0.16
	5	0.03	0.65	-0.19	0.03	0.65	0.10	0.56	-0.44	0.65	0.98	-0.38	0.03
Turbidity	1	0.04	0.04	0.04	0.04	0.04	0.04	0.04	0.04	0.04	0.04	0.16	0.16
	2	0.04	0.04	0.04	0.04	0.04	0.04	0.04	0.04	0.04	0.04	0.04	0.10
	3	0.04	0.04	0.04	0.04	0.04	0.04	0.04	0.04	0.04	0.04	0.04	0.04
	4	0.04	0.04	0.04	0.04	0.04	0.04	0.04	0.04	0.04	0.04	0.04	0.04
	5	0.04	0.04	0.04	0.04	0.04	0.04	0.04	0.04	0.04	0.10	0.04	0.04

Extended Data Fig. 9: Size and turbidity of SNP-7/8a comprising different compositions of CM conjugates.

(**a**) Table listing the properties of 20 different predicted neoantigens that were synthesized as CM conjugates and then mixed at equimolar ratios in DMSO followed by addition of PBS buffer to generate SNP-7/8a carrying 20 different CM conjugates. (**b**) Particle size and turbidity of SNP-7/8a comprising different CM conjugate compositions. The bar charts show the particle size

(gray bars; left axis) and turbidity (black bars; right axis) of 12 SNP-7/8a formulations, each containing a unique set of 5 different CM conjugates. The properties of the CM conjugates are listed in the accompanying table. Each column lists the charge and GRAVY characteristics of the neoantigens comprising each of the 5 CM conjugates comprising the particle and the turbidity value of each of the 5 CM conjugates when resuspended individually in PBS. For example, column 1 shows the size and turbidity of a particle (SNP-7/8a) comprised of 5 different CM conjugates; the 5 CM conjugates (1 through 5) are comprised of neoantigens with a net charge of –6, –4, 0, +1, and –1 and GRAVY of 0.02, –0.90, –0.13, –0.16, 0.03; and those CM conjugates (1 through 5) each have turbidity < 0.04. In columns 10–12, CM conjugates that individually are prone to form aggregates incorporate into stable nanoparticle micelles when formulated with other CM conjugates that individually form stable nanoparticle micelles.

Extended data figure 10

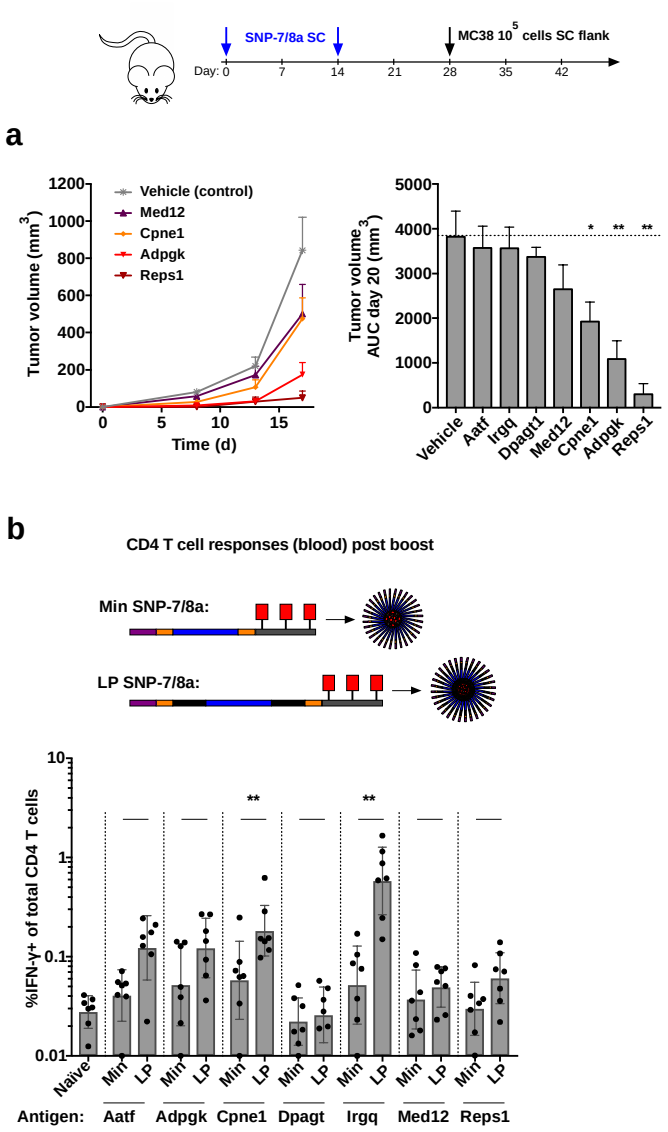

Extended Data Fig. 10: Anti-tumor efficacy and CD4 T cell immunogenicity of SNP-7/8a delivering MC38 neoantigens.
(**a**) C57BL/6 mice (*n* = 10 per group) were vaccinated subcutaneously with SNP-7/8a including different MC38 LP neoantigens or vehicle control (10% DMSO in PBS) on days 0 and 14. On day 28, mice were subcutaneously implanted with 1.0×10^5 MC38 tumor cells. Tumor growth curves (left) and area under the curve through day 20 (right) are shown. (**b**) CD4 T cell responses from blood was determined by intracellular cytokine staining on day 21 following vaccinations with SNP-7/8a delivering one of 7 MC38 neoantigens as LP or minimal epitopes. Data on log scale are reported as geometric mean with 95% c.i.; data on linear scale are reported as mean ± s.e.m. Statistical significance was determined using Kruskal-Wallis with Dunn's correction; ns = not significant, $*P < 0.05$, $**P \leq 0.01$.

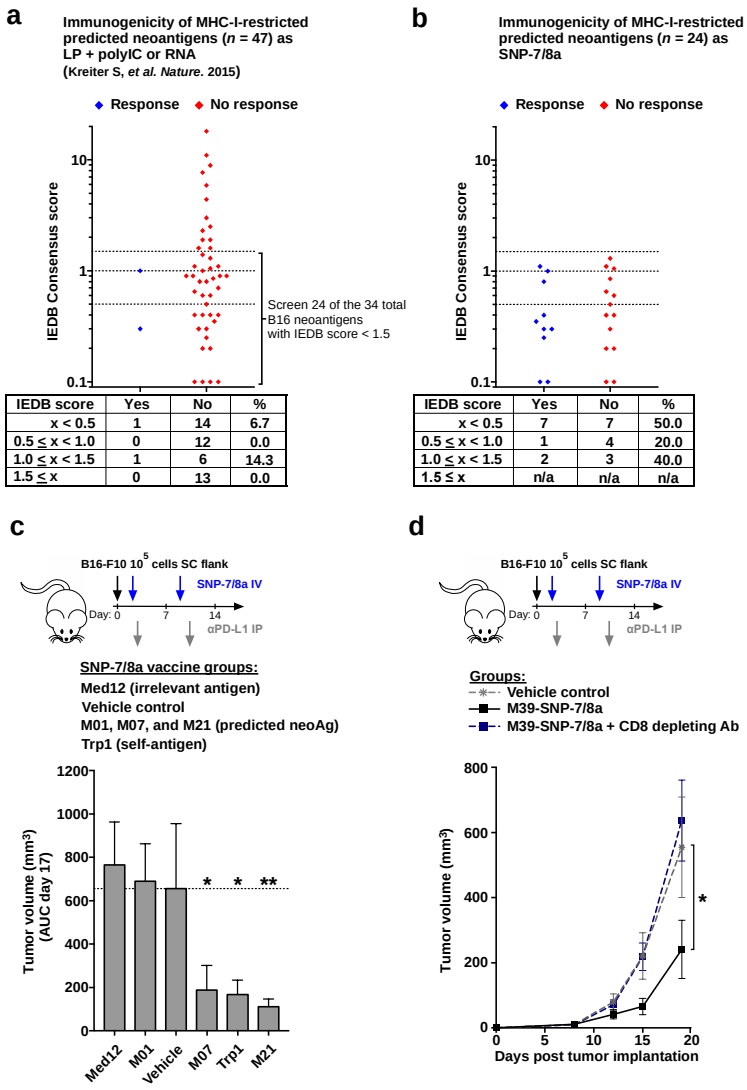

IEDB score	Yes	No	%
x < 0.5	1	14	6.7
0.5 ≤ x < 1.0	0	12	0.0
1.0 ≤ x < 1.5	1	6	14.3
1.5 ≤ x	0	13	0.0

IEDB score	Yes	No	%
x < 0.5	7	7	50.0
0.5 ≤ x < 1.0	1	4	20.0
1.0 ≤ x < 1.5	2	3	40.0
1.5 ≤ x	n/a	n/a	n/a

Extended Data Fig. 11: Immunogenicity and anti-tumor efficacy of SNP-7/8a vaccination with B16-F10 neoantigens.

(**a**) Plot of the predicted MHC-I binding affinity (IEDB consensus, any length, H2-K^b or H2-D^b) versus CD8 T cell response for B16-F10 neoantigens (*n* = 47) included in PCVs based on LP + polyIC or RNA as described (see: Kreiter *et al. Nature*, 2015). (**b**) 24 of the predicted neoantigens with moderate to high MHC-I binding affinity (IEDB consensus score < 1.5) were screened for immunogenicity *in vivo* using SNP-7/8a and the relationship between binding affinity and immunogenicity is shown. (**c**,**d**) C57BL/6 mice (*n* = 10 per group) were implanted subcutaneously with 1 × 10^5 B16-F10 cells and then vaccinated intravenously on days 1 and 8 with SNP-7/8a containing one of 4 B16-F10 LPs (M01, M07, M21, or M39) that induced a CD8 T cell response and no significant CD4 T cell response to determine whether these LPs (previously described as non-immunogenic) could mediate anti-tumor efficacy. All animals received αPD-L1 (200 μg IP) on the days indicated. (**c**) Area under the curve of tumor growth is shown for animals vaccinated with SNP-7/8a delivering the indicated antigens. (**d**) The kinetics of tumor growth following vaccination of mice with M39; an additional group of mice (*n* = 10)

vaccinated with M39 was treated with CD8 depleting antibody (250 μg IP) prior to vaccination. Data on linear scale are reported as mean ± s.e.m. Statistical significance was determined using two-way ANOVA with Bonferroni correction (**d**) or Kruskal-Wallis with Dunn's correction (**c**); ns = not significant, *$P < 0.05$, **$P \leq 0.01$.

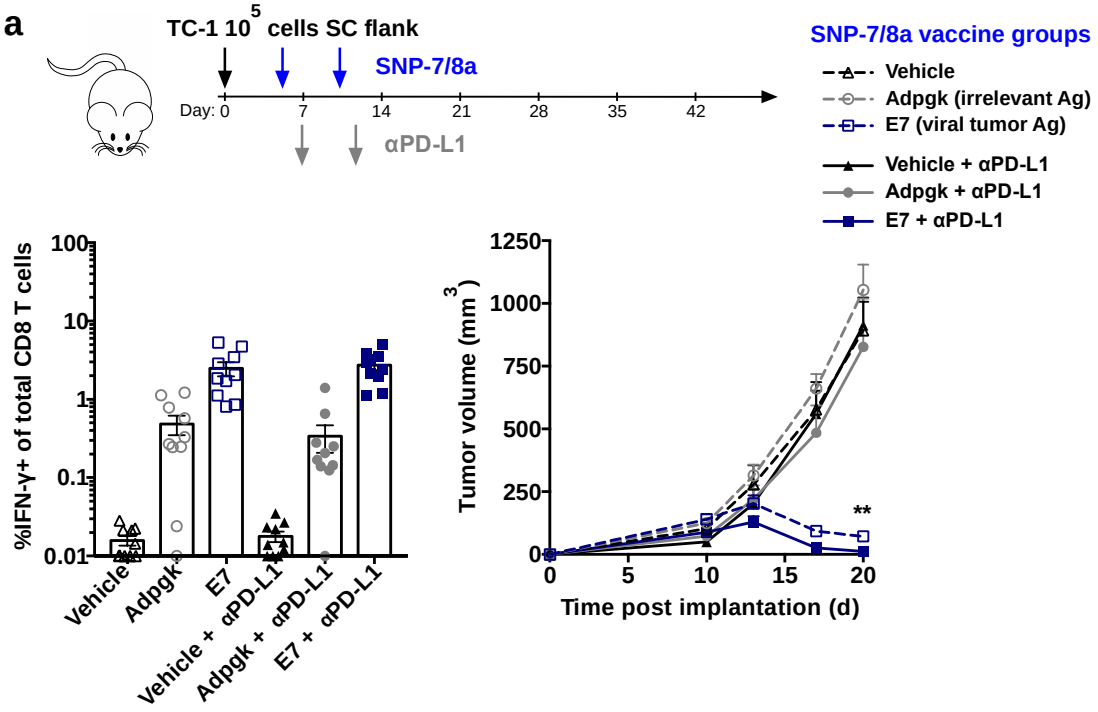

Extended Data Fig. 12: Therapeutic efficacy of SNP-7/8a delivering virus-associated tumor antigens. (**a**) C57BL/6 mice (n = 20 per group) implanted with 1.0×10^5 TC-1 tumor cells were injected subcutaneously with vehicle control (10% DMSO in PBS) or with SNP-7/8a delivering E7 from human papilloma virus or an irrelevant antigen (Adpgk neoantigen from MC38) as an inflammation control on day 0. Mice were vaccinated on days 5 and 10 after implantation. Half the animals from each group (n = 10) were treated with αPD-L1 (200 μg IP) on days 7 and 12 after implantation. CD8 T cell responses on day 12 (left) and tumor growth curves (right) are shown. Data on log scale are reported as geometric mean with 95% c.i.; data on linear scale are reported as mean ± s.e.m. Statistical significance was determined using two-way ANOVA with Bonferroni correction; ns = not significant, *$P < 0.05$, **$P \leq 0.01$.

Extended Data Table 1: Immunogenic B16-F10 mutations (CD8 responses)

Mutation	Mutated sequence	Predicted MHC-I epitope	IEDB score	Published CD8 response*		Present study	
				RNA	LP + polyIC	Screened	SNP-7/8a
B16-M34	HLTQQLDTYILKNVVAFSRTDKYRQLP	VVAFSRTDKYRQL	0.1			×	
B16-M49	EKFSMDHKTGTIAMQNTTQLRSRYELT	HKTGTIAMQNTTQL	0.1			×	
B16-M05	FVVKAYLPVNESFAFTADLRSNTGGQA	LPVNESFAFTADL	0.1			×	×
B16-M39	ELINFKRKRVAAFQKNLIEMSELEIKH	RVAAFQKNLIEM	0.1			×	×
B16-M26	RVDQKTLHNLLRKVVPSFSAEIERLNQ	RKVVPSFSAEIERL	0.2			×	
B16-M44	EFKHIKAFDRTFANNPGPMVVFATPGM	FANNPGPM	0.2			×	
B16-M21	SSPDEVALVEGVQSLGFTYLRLKDNYM	QSLGFTYL	0.25			×	×
B16-M07	TAKSVMCTYSPPLDKLFCQLAKTCPVQ	SVMCTYSPPLDK	0.3			×	×
B16-M37	GPDGLALPNNYCDVCLGDSKINKKTGQ	LALPNNYCDV	0.3			×	
B16-M33	DSGSPFPAAVILRDALHMARGLKYLHQ	AAVILRDAL	0.3	×		×	×
B16-M01	SGCYFMVAVAHVAAFLLEDRAVCVERF	VAVAHVAAFL	0.35			×	×
B16-M17	VVDRNPQFLDPVLAYLMKGLCEKPLAS	RNPQFLDPVLAYL	0.4			×	
B16-M36	CGTAFFINFIAIYHHASRAIPFGTMVA	IAIYHHASRAIPF	0.4			×	
B16-M25	STANYNTSHLNNDVWQIFENPVDWKEK	SHLNNDVWQI	0.4			×	×
B16-M40	NREKMKGELGMMLILQNVIQKTTTPGE	MMLILQNVI	0.5			×	
B16-M29	IPSGTTILNCFHDVLSGKLSGGSPGVP	GTTILNCFHDVL	0.6			×	
B16-M46	NHSGLVTFQAFIDVMSRETTDTDTADQ	VTFQAFIDVMS	0.65			×	
B16-M47	GRGHLLGRLAAIVGKQVLLGRKVVVVR	AAIVGKQVL	0.8			×	×
B16-M23	LILISTNGSFIRLLDAFKGVVMHTFGG	TNGSFIRLL	0.85			×	
B16-M27	REGVELCPGNKYEMRRHGTTHSLVIHD	GVELCPGNKYEM	1	×	×	×	×
B16-M19	NEVAPLEWLRYFDKKELELMLCGMQEI	EWLRYFDKKEL	1.05			×	
B16-M30	PSKPSFQEFVDWENVSPELNSTDQPFL	NVSPELNSTDQPFL	1.1			×	
B16-M08	ANFESGKHKYRQTAMFTATMPPAVERL	AMFTATMPPAVERL	1.1			×	×
B16-M22	PKPDFSQLQRNILPSNPRVTRFHINWD	DFSQLQRNILPS	1.3			×	
B16-M20	FRRKAFLHWYTGEAMDEMEFTEAESNM	KAFLHWYTGEAM	0.4				
B16-M38	SCTEGQISIAKYENCPKDNPMYYCNKK	AKYENCPKDNPM	0.6				
B16-M35	LVLSFVGQTRVLMINGEEVEETELMGF	VLMINGEEV	0.7				
B16-M02	NQGAENVEQVLVTSIQGAVDYPDPIAQ	VTSIQGAVDYPDPI	0.8				
B16-M03	MTESFKKKFEECQHNIIKLQNGHTSLA	QHNIIKLQNGHTSL	0.9				
B16-M10	RGQSQLFSLNPRGRSLVTAGRIDREEL	QSQLFSLNPRGRSL	0.9				
B16-M11	ASSSLARGPLSEAGLALFDPYSKEEST	SSLARGPLSEAGL	0.9				
B16-M14	AVTYAAQQHETFLTNGDRAGFLIGDGA	VTYAAQQHETFLT	0.9				
B16-M48	SHCHWNDLAVIPAGVVHNWDFEPRKVS	AGVVHNWDFEPRKV	1				
B16-M45	ECRITSNFVIPSEYWVEEKEEKQKLIQ	SNFVIPSEYWVEE	1.4				
B16-M28	NIEGIDKLTQLKKPFLVNNKINKIENI	PFLVNNKINKIENI	1.6				
B16-M31	DNIPALVEEYLERGNFVANDLDWLLAL	GNFVANDLDWLLAL	1.6				
B16-M09	QRAAAPSAASSPADVQSLKKAMSSLQN	ADVQSLKKAMSSL	1.9				
B16-M12	TPPPEEAMPFEFNGPAQGDHSQPPLQV	PEEAMPFEFNGPA	1.9				
B16-M32	EATELKACKPNGKRNPYCEVSMGSQSY	NGKRNPYCEV	2.3				
B16-M50	GFSQPLRRLVLHVVSAAQAERLARAEE	VLHVVSAAQAERL	2.5				
B16-M41	HSLSIECKGIDKEINESKNTHLDIPRI	INESKNTHL	3				
B16-M13	KFRLTASNMEGKSWPSEVLVCTTSPDR	KSWPSEVL	4.4				
B16-M24	TAVITPPTTTTKKARVSTPKPATPSTD	ITPPTTTTKKARV	5.9				
B16-M06	PDVHTLLEITEESGAVLVDKSDSD	ITEESGAV	7.65				
B16-M16	RVTCNRAGEKHCFSSNEAARDFGGAIQ	SSNEAARDFGGAI	8.9				
B16-M04	PRVSALIESLNQKTQSTGDHPQPTDTT	SALIESLNQKTQ	11				
B16-M18	VETLECERGKQEAKLLAERSRFEDEKQ	KLLAERSRF	18.1				
B16-M42	#						
B16-M43	#						
B16-M15	#						

*Kreiter S, *et al*. *Nature* (2015); #sequence not found

Extended Data Table 2: Immunogenic B16-F10 mutations (CD4 responses)

Mutation	Mutated sequence	Predicted MHC-II epitope	IEDB score	Published CD4 response*		Present study	
				LP + polyIC	RNA	Screened	SNP-7/8a
B16-M34	HLTQQLDTYILKNVVAFSRTDKYRQLP	DTYILKNVVAFSRTD	21.37			×	
B16-M49	EKFSMDHKTGTIAMQNTTQLRSRYELT	MDHKTGTIAMQNTTQ	32.48			×	
B16-M05	FVVKAYLPVNESFAFTADLRSNTGGQA	VKAYLPVNESFAFTA	10.16	×		×	×
B16-M39	ELINFKRKRVAAFQKNLIEMSELEIKH	RKRVAAFQKNLIEMS	21.91			×	
B16-M26	RVDQKTLHNLLRKVVPSFSAEIERLNQ	NLLRKVVPSFSAEIE	6.12			×	
B16-M44	EFKHIKAFDRTFANNPGPMVVFATPGM	FDRTFANNPGPMVVF	6.61	×	×	×	×
B16-M21	SSPDEVALVEGVQSLGFTYLRLKDNYM	EVALVEGVQSLGFTY	47.12		×	×	
B16-M07	TAKSVMCTYSPPLDKLFCQLAKTCPVQ	KSVMCTYSPPLDKLF	16.92			×	
B16-M37	GPDGLALPNNYCDVCLGDSKINKKTGQ	GPDGLALPNNYCDVC	63.43			×	
B16-M33	DSGSPFPAAVILRDALHMARGLKYLHQ	DSGSPFPAAVILRDA	8.37			×	×
B16-M01	SGCYFMVAVAHVAAFLLEDRAVCVERF	SGCYFMVAVAHVAAF	2.23			×	
B16-M17	VVDRNPQFLDPVLAYLMKGLCEKPLAS	VDRNPQFLDPVLAYL	19.75	×		×	×
B16-M36	CGTAFFINFIAIYHHASRAIPFGTMVA	FIAIYHHASRAIPFG	7.52	×		×	
B16-M25	STANYNTSHLNNDVWQIFENPVDWKEK	STANYNTSHLNNDVW	13.05	×	×	×	×
B16-M40	NREKMKGELGMMLILQNVIQKTTTPGE	LILQNVIQKTTTPGE	40.53			×	
B16-M29	IPSGTTILNCFHDVLSGKLSGGSPGVP	DVLSGKLSGGSPGVP	10.55	×		×	
B16-M46	NHSGLVTFQAFIDVMSRETTDTDTADQ	LVTFQAFIDVMSRET	33.91	×	×	×	×
B16-M47	GRGHLLGRLAAIVGKQVLLGRKVVVVR	GRGHLLGRLAAIVGK	35.75		×	×	
B16-M23	LILISTNGSFIRLLDAFKGVVMHTFGG	IRLLDAFKGVVMHTF	21.82			×	×
B16-M27	REGVELCPGNKYEMRRHGTTHSLVIHD	KYEMRRHGTTHSLVI	31.81			×	
B16-M19	NEVAPLEWLRYFDKKELELMLCGMQEI	LEWLRYFDKKELELM	66.41			×	
B16-M30	PSKPSFQEFVDWENVSPELNSTDQPFL	EFVDWENVSPELNST	18.92	×	×	×	×
B16-M08	ANFESGKHKYRQTAMFTATMPPAVERL	TAMFTATMPPAVERL	0.14		×	×	×
B16-M22	PKPDFSQLQRNILPSNPRVTRFHINWD	LQRNILPSNPRVTRF	4.9	×		×	×
B16-M20	FRRKAFLHWYTGEAMDEMEFTEAESNM			×			
B16-M38	SCTEGQISIAKYENCPKDNPMYYCNKK						
B16-M35	LVLSFVGQTRVLMINGEEVEETELMGF						
B16-M02	NQGAENVEQVLVTSIQGAVDYPDPIAQ						
B16-M03	MTESFKKKFEECQHNIIKLQNGHTSLA						
B16-M10	RGQSQLFSLNPRGRSLVTAGRIDREEL						
B16-M11	ASSSLARGPLSEAGLALFDPYSKEEST						
B16-M14	AVTYAAQQHETFLTNGDRAGFLIGDGA						
B16-M48	SHCHWNDLAVIPAGVVHNWDFEPRKVS			×	×		
B16-M45	ECRITSNFVIPSEYWVEEKEEKQKLIQ			×			
B16-M28	NIEGIDKLTQLKKPFLVNNKINKIENI			×	×		
B16-M31	DNIPALVEEYLERGNFVANDLDWLLAL						
B16-M09	QRAAAPSAASSPADVQSLKKAMSSLQN						
B16-M12	TPPPEEAMPFEFNGPAQGDHSQPPLQV			×			
B16-M32	EATELKACKPNGKRNPYCEVSMGSQSY						
B16-M50	GFSQPLRRLVLHVVSAAQAERLARAEE			×	×		
B16-M41	HSLSIECKGIDKEINESKNTHLDIPRI						
B16-M13	KFRLTASNMEGKSWPSEVLVCTTSPDR						
B16-M24	TAVITPPTTTTKKARVSTPKPATPSTD			×			
B16-M06	PDVHTLLEITEESGAVLVDKSDSD						
B16-M16	RVTCNRAGEKHCFSSNEAARDFGGAIQ						
B16-M04	PRVSALIESLNQKTQSTGDHPQPTDTT						
B16-M18	VETLECERGKQEAKLLAERSRFEDEKQ						
B16-M42	#						
B16-M43	#						
B16-M15	#						

*Kreiter S, *et al*. *Nature* (2015); #sequence not found